

# Firing Patterns of Cerebellar Purkinje Cells During Locomotion and Sleep

Britton Sauerbrei

In Partial Fulfillment of the Requirements  
for the Degree of  
Doctor of Philosophy

California Institute of Technology  
Pasadena, California

2016  
Defended November 18th, 2015

© 2015

Britton Sauerbrei

All rights reserved

*To my parents.*

## Acknowledgements

My scientific and personal development over the past six years owes a tremendous debt to my advisor, Thanos Siapas. His mentorship at the bench, command prompt, and seminar table, and his dedication to excellence in engineering, experiment, analysis, and communication, have profoundly shaped my work and life. Furthermore, the intellectual independence he offered throughout my graduate career allowed me to totally focus my mind, hands, and time on cerebellar cortex and to pursue my ideas wherever they led. I'll never forget the first Purkinje cell we recorded or the flood of exuberance that followed.

For their guidance and discussions, I would like to thank my thesis committee, including Richard Andersen, for sparking my interest in motor systems during my first year at Caltech; Michael Dickinson, for an ethological perspective and invaluable feedback on the locomotion project; Pietro Perona, for mentorship and a computational point of view; and Paul Sternberg, for insight and encouragement. I also wish to thank Gilles Laurent, whose scientific example and advice have influenced me deeply, and David Anderson, whose graduate seminar served as an outstanding introduction to current techniques in neurobiology, and as a springboard for many stimulating discussions.

I would like to thank my colleagues in the Siapas lab, whose help and camaraderie have made the years in Beckman Institute such a pleasure: Casimir Wierzynski, for teaching me the art of tetrode recording and the science of rat whispering; Eugene Lubenov, for always encouraging me to dig just a little deeper into the data; Maria Papadopoulou, for great patience in helping me with histology; Stijn Cassenaer, for scientific and professional advice; Laurent Moreaux, for many lively conversations; Kevin Shan, for technical wizardry in the measurement of head attitude and beyond, and for humoring my coffee tasting terms during our quest for the perfect shot; Brad Hulse, for his formidable experimental

prowess, Midwestern good humor, and company at countless ham-and-cheese lunches; Andreas Hoenselaar, for wry wit and the contribution of elegant, powerful, and indispensable software; Gustavo Rios, for frequent printer-side chats and for setting the bar with his work ethic; Koichiro Kajikawa, for keeping the ball rolling; and Jennifer Mok, for bringing good cheer and delicious Chinese sweets into the lab.

This thesis would have been impossible without the tireless support of my family and my friends at Caltech. I thank Federico Tadei, for years of domestic bliss, the secret to puttanesca sauce (forever safe!), and Mozart sing-alongs; Bill Fefferman, for his steady hand at the espresso machine and pool table and his impeccable taste in painting and Cabernet Franc; Niranjan Srinivas, for sustaining the spirit of CNS, guiding me through the rough patches, and leading me to the finest Carnatic concerts in Southern California; Subhonmesh Bose, for the Hindustani blues and a big heart; Aditya Kher, for his infectious California cool; Tejaswi Venumadhav, for mind-bending conversations; and Murat Koloğlu, for a never-dull year at one-ninety-two.

Finally, I wish to express my indebtedness to the multitude of researchers whose investigations into the anatomy and physiology of nervous systems continue to instruct, to guide, and to inspire; faced with such a body of work, the student glows while he reads, but trembles as he writes.

## Abstract

The cerebellum is a major supraspinal center involved in the coordination of movement. The principal neurons of the cerebellar cortex, Purkinje cells, receive excitatory synaptic input from two sources: the parallel and climbing fibers. These pathways have markedly different effects: the parallel fibers control the rate of simple sodium spikes, while the climbing fibers induce characteristic complex spike bursts, which are accompanied by dendritic calcium transients and play a key role in regulating synaptic plasticity. While many studies using a variety of species, behaviors, and cerebellar regions have documented modulation in Purkinje cell activity during movement, few have attempted to record from these neurons in unrestrained rodents. In this dissertation, we use chronic, multi-tetrode recording in freely-behaving rats to study simple and complex spike firing patterns during locomotion and sleep. Purkinje cells discharge rhythmically during stepping, but this activity is highly variable across steps. We show that behavioral variables systematically influence the step-locked firing rate in a step-phase-dependent way, revealing a functional clustering of Purkinje cells. Furthermore, we find a pronounced disassociation between patterns of variability driven by the parallel and climbing fibers, as well as functional differences between cerebellar lobules. These results suggest that Purkinje cell activity not only represents step phase within each cycle, but is also shaped by behavior across steps, facilitating control of movement under dynamic conditions. During sleep, we observe an attenuation of both simple and complex spiking, relative to awake behavior. Although firing rates during slow wave sleep (SWS) and rapid eye movement sleep (REM) are similar, simple spike activity is highly regular in SWS, while REM is characterized by phasic increases and pauses in simple spiking. This phasic activity in REM is associated with pontine waves, which propagate into the cerebellar cortex and modulate both simple and complex spiking. Such a tempo-

ral coincidence between parallel and climbing fiber activity is known to drive plasticity at parallel fiber synapses; consequently, pontocerebellar waves may provide a mechanism for tuning synaptic weights in the cerebellum during active sleep.

## Published Content and Contributions

Chapter 3 has been modified from Sauerbrei, Lubenov, & Siapas (2015), and a manuscript based on Chapter 4 is in preparation for submission. In both studies, I contributed to the experimental design, data collection, statistical analysis, interpretation of results, figure design, and writing.

Sauerbrei, B.A., Lubenov, E.V., and Siapas, A.G. (2015). Structured Variability in Purkinje Cell Activity during Locomotion. *Neuron* 87, 840-852.

doi:10.1016/j.neuron.2015.08.003

# Contents

<b>Acknowledgements</b>	<b>iv</b>
<b>Abstract</b>	<b>vi</b>
<b>Published Content and Contributions</b>	<b>viii</b>
<b>List of Figures</b>	<b>x</b>
<b>1 Introduction</b>	<b>1</b>
<b>2 Multi-Tetrode Recording in the Cerebellar Cortex of Unrestrained Rats</b>	<b>10</b>
<b>3 Structured Variability in Purkinje Cell Activity during Locomotion</b>	<b>19</b>
3.1 Summary . . . . .	19
3.2 Introduction . . . . .	19
3.3 Results . . . . .	25
3.4 Discussion . . . . .	39
3.5 Experimental Procedures . . . . .	48
<b>4 State-Dependent Firing Patterns in Cerebellar Purkinje Cells during Sleep</b>	<b>54</b>
4.1 Summary . . . . .	54
4.2 Introduction . . . . .	54
4.3 Results . . . . .	56
4.4 Discussion . . . . .	62
4.5 Experimental Procedures . . . . .	64
<b>References</b>	<b>66</b>

## List of Figures

1	Cerebellar morphology and microcircuit. . . . .	2
2	Some mossy fiber pathways into the cerebellum . . . . .	5
3	Instrumentation. . . . .	11
4	Histology. . . . .	13
5	Single units recorded in cerebellar cortex. . . . .	16
6	Experimental setup and behavior . . . . .	21
7	Firing rates during walking and licking. . . . .	23
8	A single lap across the track. . . . .	26
9	Purkinje cell activity is rhythmic, but variable. . . . .	27
10	Patterns of step-to-step variability. . . . .	30
11	Behavior modulates step-to-step variability. . . . .	32
12	Behavioral modulation depends strongly on step phase. . . . .	35
13	Step-to-step variability is correlated across Purkinje cells. . . . .	37
14	Complex spike tuning within and across steps. . . . .	38
15	Purkinje cell properties differ across cerebellar lobules. . . . .	40
16	A dynamic view of neuronal activity during locomotion. . . . .	41
17	Purkinje cell recording during sleep. . . . .	58
18	State-dependent simple and complex spike rates. . . . .	59
19	Detection of pontocerebellar waves. . . . .	61
20	Purkinje cell modulation during pontocerebellar waves. . . . .	62

# 1 Introduction

*And what I write I cast upon the stream,  
To swim or sink — I have had at least my dream.  
- Byron, Don Juan*

The cerebellum can be distinguished in all vertebrates except hagfish (Nieuwenhuys et al., 1998). In lampreys, it consists of a small ridge of tissue posterior to the optic tectum, receiving afferents mainly from the vestibular and lateral line nerves, though projections from the spinal cord and other sources are present, as well (Larsell and Jansen, 1967). The cerebellar cortex is well defined in sharks and rays, and its principal neurons, the Purkinje cells, project to a series of deep nuclei. This organization has been preserved throughout vertebrate phylogeny, despite extensive morphological variation (Figure 1A). The cerebellum is prominent in bony fish, and it is greatly enlarged in Mormyridae, a family of weakly electric fish, where it covers the entire dorsal surface of the brain. Amphibians, by contrast, have a reduced cerebellum. In birds and mammals, the cortex has a large surface area, and is folded rostrocaudally into lobules (Figure 1A, B). Afferent fibers carrying a diverse range of sensory signals reach the cerebellum, and these often suggest a role in the control of the orientation of the head, body, and limbs: in turtles, for instance, a prominent disynaptic retinocerebellar pathway overlaps with vestibular projections (Reiner and Karten, 1978), the lateral line system supplies a major projection in fish, and the mammalian cerebellum receives extensive proprioceptive and vestibular signals. As the cerebral hemispheres expanded in mammalian evolution, cerebellar areas with bidirectional, polysynaptic connections to the neocortex exhibited a corresponding enlargement.

The cerebellar cortex of mammals has a highly stereotyped architecture, consisting of three layers: the deep granule cell layer, the superficial molecular layer, and the inter-

Figure 1: Cerebellar morphology and microcircuit. (Continued on the following page)

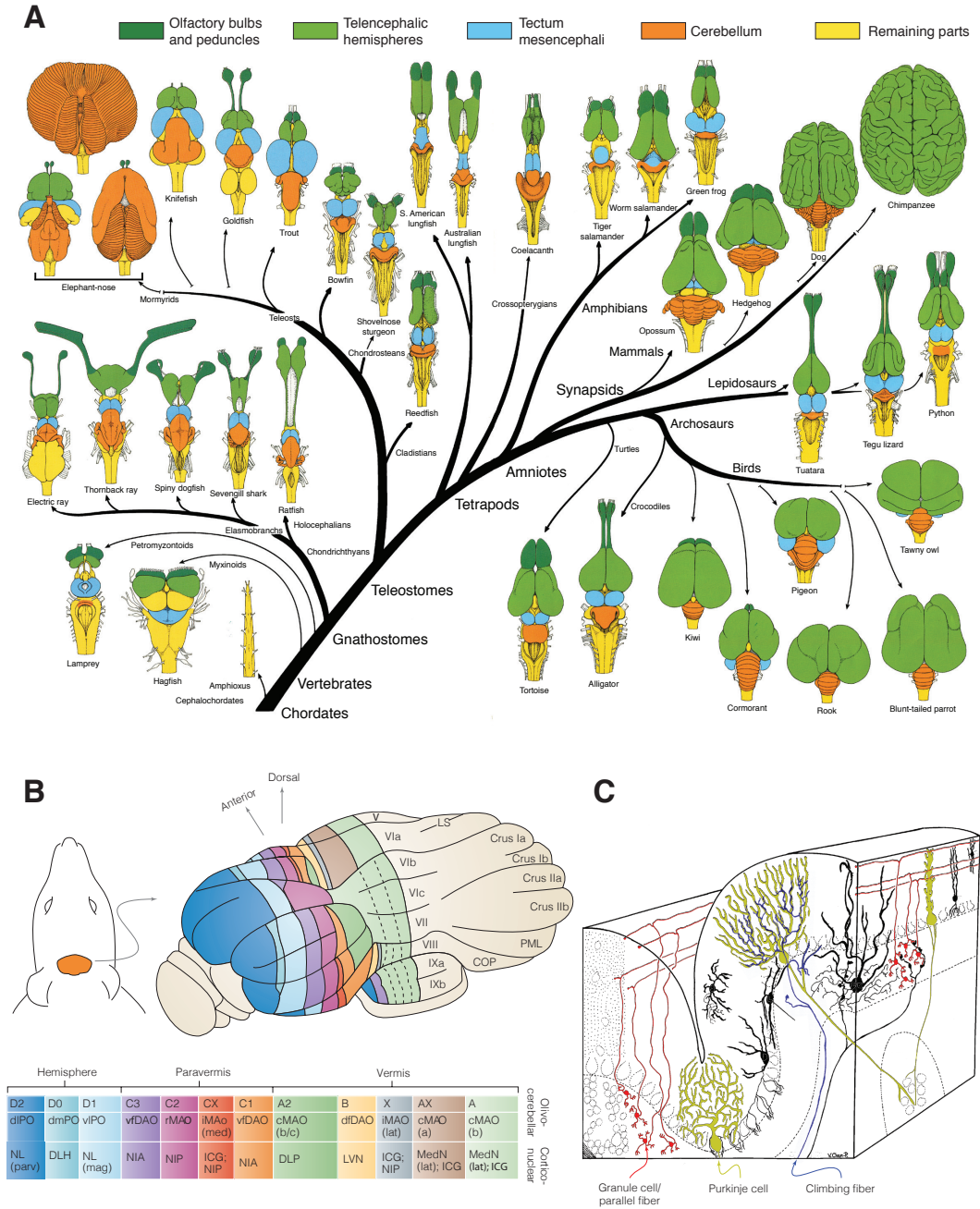


Figure 1: **(A)** Dorsal views of the brains of selected vertebrates, from Nieuwenhuys, ten Donkelaar, and Nicholson (1998), illustrating the extensive variation in the size and gross morphology of the cerebellum (orange). **(B)** Longitudinal zones in the rat cerebellum, defined by white matter compartments, olivocerebellar projections, corticonuclear projections, gene expression patterns, and physiological responses in the climbing fibers; from Apps and Hawkes (2009). Rat head re-drawn from Greene (1968). **(C)** The cerebellar microcircuit, adapted from Palay and Chan-Palay (1974). Purkinje cells (yellow) are the principal neurons of the cerebellar cortex, and receive excitatory input from the parallel fibers of granule cells (red), and from the climbing fibers of the inferior olive (blue).

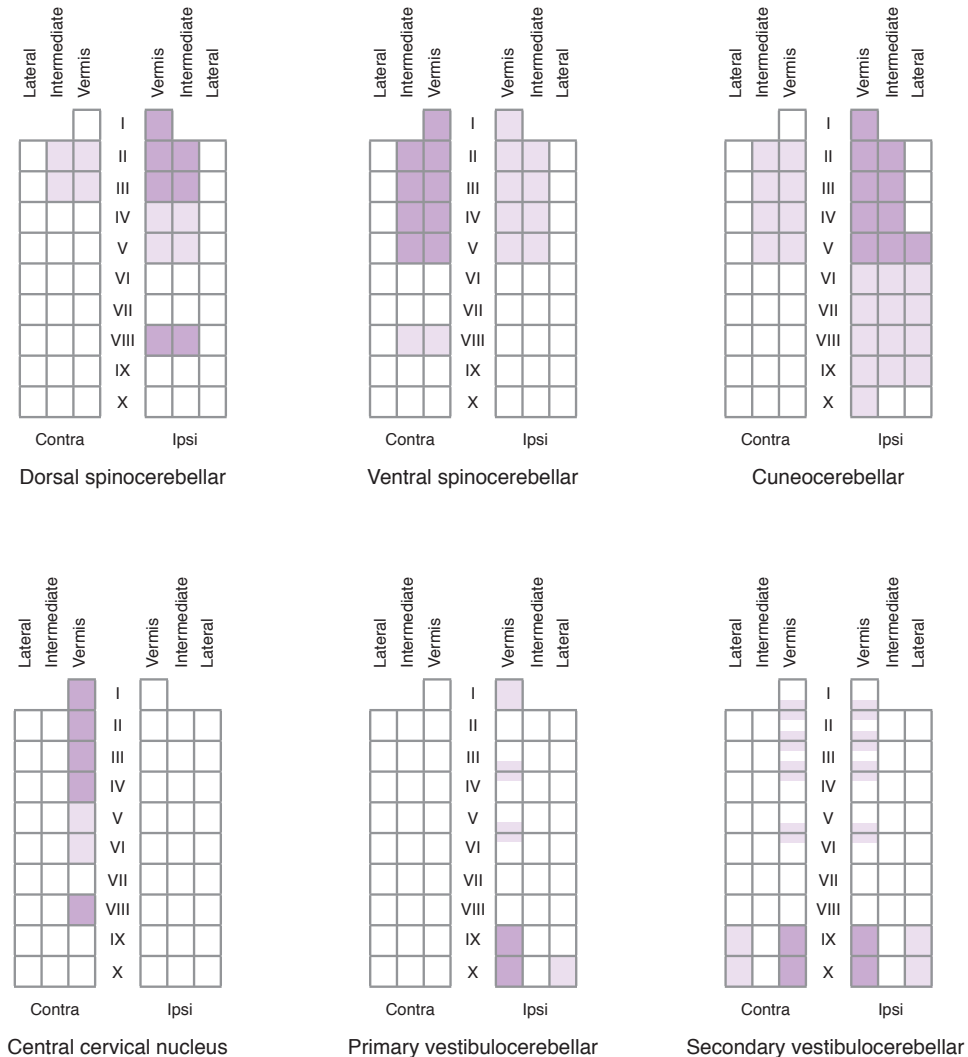
mediate Purkinje cell layer, where the cell bodies of the GABAergic principal neurons are concentrated (Figure 1C). Purkinje cells have extensive dendritic arbors which are flattened in the sagittal plane and receive excitatory synaptic input from two sources: the parallel fibers and the climbing fibers. The parallel fibers arise from cerebellar granule cells, which integrate 4-6 synaptic inputs from mossy fibers originating in the spinal cord, brainstem, or vestibular nerve. Granule cells send their axons to the molecular layer, where they bifurcate and run several millimeters mediolaterally. Tens of thousands of parallel fibers — perhaps as many as 200,000 in the rat — synapse onto each Purkinje cell, providing weak excitation (Barbour, 1993) and regulating the rate of sodium action potentials, or simple spikes. The climbing fibers, by contrast, originate in the contralateral inferior olive. Each Purkinje cell is contacted by a single climbing fiber, which forms thousands of synapses on its dendritic tree. Activation of the climbing fiber induces a complex spike, which consists of a burst of high-frequency, axonally-generated spikelets, along with a large dendritic calcium transient (Davie et al., 2008; Eccles et al., 1966; Kitamura and Hausser, 2011). Complex spikes are followed by a pause in simple spiking, mediated by calcium-dependent potassium channels (Rancz and Husser, 2010), and often by a brief rebound in the simple spike rate after this pause.

Because complex spikes occur at much lower rates than simple spikes, and because the burst of spikelets does not propagate down the axon (Monsivais et al., 2005), the climbing

fiber system probably has little direct effect on the firing rates of postsynaptic nuclear neurons. However, this system plays a key role in synaptic plasticity: repeated pairing of climbing and parallel fiber stimulation induces long-term depression at parallel fiber synapses (Ito, 2001). This depression is complemented by long-term potentiation resulting from low-frequency, unpaired parallel fiber stimulation (Crepel and Jaillard, 1991), as well as by other forms of plasticity (Hansel et al., 2001). It has been suggested that the cerebellar cortex implements a perceptron-like computation, in which the climbing fibers carry an error signal used to tune parallel fiber synaptic weights, allowing the system to learn a target transfer function and reduce motor errors (Albus, 1971; Marr, 1969).

The mossy and climbing fiber afferents to the cerebellar cortex are precisely and topographically organized (Apps and Hawkes, 2009). Early studies divided the cerebellum into three main zones (Goodman and Simpson, 1961; Jansen and Brodal, 1940): a medial, vermal area, projecting to the fastigial nucleus, an intermediate region, or paravermis, connected with the interposed nuclei, and the lateral hemispheres, projecting to the dentate nucleus. In addition, the flocculus and nodulus were identified as vestibular areas on the basis of fiber connections. Subsequent work has revealed a much finer partition. Longitudinal zones, which run parasagittally (Figure 1B), are defined by the coincidence of several structural and functional boundaries. First, the cerebellar white matter is partitioned into compartments, which can be revealed by acetylcholinesterase staining. Second, climbing fiber projections from a given subnucleus of the inferior olive terminate in a narrow, parasagittal strip (Groenewegen and Voogd, 1977). Third, Purkinje cells in an olivary terminal zone project to a specific target in the deep cerebellar nuclei; critically, the boundaries in the corticonuclear projections coincide with those of the olivocerebellar projections. Fourth, the anatomical boundaries correspond to boundaries in climbing fiber somatosen-

Figure 2: Some mossy fiber pathways into the cerebellum (layout based on Roberts, 1967). The grid partitions the cerebellar cortex mediolaterally (into the vermis, the intermediate regions, and the lateral regions) and rostrocaudally (into lobules). Lateral portions of IX and X correspond to the paraflocculus and flocculus, respectively. Purple shading denotes a documented projection, with lighter shading for sparser projections. Based upon studies in rodents, where possible. Data for dorsal and ventral spinocerebellar tracts may be found in Anderson (1943; rats), Jansen and Brodal (1954; survey), Oscarsson (1965; survey), Snyder, Faull, and Mehler (1978; rats), Matsushita and Hosoya (1979; rats), Paxinos (2004; rats), Hantman and Jessell (2010; mice). Cuneocerebellar: Tolbert and Gutting (1997; rats), Alisky and Tolbert (1997; rats), Ji and Hawkes (1994; rats), Huang et al (2013; mice). Central cervical nucleus: Snyder, Faull, and Mehler (1978; rats), Matsushita and Hosoya (1979; rats), Matsushita and Tanami (1987; cats). Primary vestibulocerebellar: Kotchabhakdi and Walberg (1978; cats), Gerrits et al (1989; rabbits), Barmack et al (1993; rabbits). Secondary vestibulocerebellar: Barmack et al (1992; rats and rabbits). A number of other important pathways (e.g. from the basilar pontine nuclei) are not depicted.



sory receptive fields (Oscarsson, 1979); the partition imposed by receptive field mapping, however, is finer than that arising from anatomical studies. Finally, these zones are typically in register with boundaries in the expression of Zebrin II / Aldolase C, an enzyme involved in glycolysis (Brochu et al., 1990; Fujita et al., 2014; Hawkes et al., 1985).

The projection patterns of mossy fibers are somewhat more diffuse than those of the climbing fibers. A number of spinocerebellar, pontocerebellar, and vestibulocerebellar mossy fiber projections reach the cerebellum (e.g., Figure 2), and a coarse topographical organization is present across the vermis, with pathways from the tail, hindlimbs, forelimbs, and head distributed to successively more posterior regions (Dow and Moruzzi, 1958; Larsell and Jansen, 1967). On a finer spatial scale, a fractured somatotopy has been revealed by microelectrode mapping of somatosensory receptive fields, with abrupt discontinuities between patches (Shambes et al., 1978). Furthermore, the termination of mossy fibers tends to roughly coincide with longitudinal zones (Apps and Hawkes, 2009; Gravel and Hawkes, 1990; Ji and Hawkes, 1994; Voogd et al., 2003).

The cerebellum is not required for the initiation of movement, but is critical for the smoothness, speed, and precision of execution. Several lines of evidence have clearly established the role of the structure in motor control. First, the cerebellum has extensive and bidirectional connections with motor systems in the spinal cord and brainstem. Second, damage to the cerebellum disrupts effective movement (Dow and Moruzzi, 1958). In dogs and cats, cerebellar ablation results in an abnormal posture in which the forelimbs are rigidly extended and the neck is dorsiflexed, and in severe motor deficits. Animals can recover from some of these acute effects and are eventually able to stand and walk, but still suffer from dysmetria, decomposition of movement, gait abnormalities, and other symptoms. On the other hand, sensory capabilities, the initiation of voluntary movement, and

higher functions appear to be essentially unaffected following cerebellar damage. Third, stimulation of the cerebellum evokes or modulates movements. Early studies established that electrical stimulation of the cerebellar cortex relieves decerebrate rigidity (Sherrington, 1897) and elicits several characteristic postures, which vary systematically with the location of the stimulus (Chambers and Sprague, 1955; Goodman and Simpson, 1961). More recently, cell-type-specific optogenetic manipulation of Purkinje cells has been shown to induce specific limb movements (Lee et al., 2015) that depend on behavioral state (Hoogland et al., 2015). Fourth, the firing of cerebellar neurons is strongly modulated by movement. Single-unit microelectrode recordings in awake animals have revealed changes in Purkinje cell firing rates during a wide variety of behaviors, such as reaching (Thach, 1968), smooth pursuit eye movement (Lisberger and Fuchs, 1978), and licking (Cao et al., 2012). Typically, simple spiking is robustly tuned to movement parameters such as direction and speed; by contrast, complex spiking often exhibits more subtle stimulus tuning, but may modulate patterns of simple spikes (Barmack and Yakhnitsa, 2003; Medina and Lisberger, 2008).

The cerebellum plays a critical role in the coordination of locomotion. Its contribution has been studied extensively in the hindlimb regions of the vermis and paravermis of decerebrate cats, in which locomotion can be evoked by stimulation of a site in the midbrain (Shik et al., 1966). Several ascending pathways carry information into the cerebellar cortex during locomotion. The neurons of the dorsal spinocerebellar tract (DSCT) lie in Clarke's column and project to the ipsilateral cerebellar cortex, and they receive monosynaptic excitation from muscle spindles and Golgi tendon organs (Eccles et al., 1961; Lundberg and Oscarsson, 1956; Oscarsson, 1965). These cells respond strongly during both active and passive movements of the hindlimb (Arshavsky et al., 1986), and appear to represent global limb parameters, rather than the state of a single joint (Bosco and Poppele, 2001). Dur-

ing stepping, DSCT neurons discharge rhythmically, but this modulation is abolished by deafferentation; thus, the tract is believed to relay sensory information about the state of the limbs to cerebellar cortex. Recent studies, however, have questioned the idea that the tract is strictly a sensory relay: intracellular recordings during fictive locomotion, in the absence of sensory drive, have demonstrated rhythmic modulation in many DSCT neurons (Fedirchuk et al., 2013; Stecina et al., 2013), and direct excitatory connections from corticospinal neurons have been documented in mice (Hantman and Jessell, 2010). The ventral spinocerebellar tract (VSCT) originates in cells along the ventrolateral border or in the intermediate zone of the gray matter. Like DSCT neurons, cells of the VSCT receive monosynaptic excitation from spindles (Lundberg and Weight, 1971) and discharge rhythmically during locomotion. This modulation persists after deafferentation, however, and the VSCT is thought to carry signals from the spinal central pattern generator into the cerebellum; such signals appear to be present in a pathway from the reticular formation, as well (Arshavsky et al., 1986; Orlovsky et al., 1999). While the majority of physiological studies have focused on hindlimb areas, the forelimbs appear to be served by similar systems, including the cuneocerebellar and rostral spinocerebellar tracts; little is known about their role in motor control, however (Alisky and Tolbert, 1997; Huang et al., 2013; Ji and Hawkes, 1994; Oscarsson, 1965; Oscarsson and Uddenberg, 1964; Tolbert and Gutting, 1997).

Purkinje cells in the limb areas, as well as their postsynaptic targets in the cerebellar and vestibular nuclei, discharge rhythmically during locomotion. The step tuning properties of Purkinje cells are diverse: each cell fires most intensely at a specific step phase, but across the population, the preferred phases span the entire cycle, though the distribution of preferred phases is non-uniform. This modulation not only reflects sensory input, but appears

to be under central control, as well: during fictive scratching, contralateral hemisection of the spinal cord, which interrupts the VSCT, abolishes rhythmic activity in Purkinje cells (Arshavsky et al., 1984). Furthermore, Purkinje cells shape the activity of descending pathways: vestibulospinal, reticulospinal, and rubrospinal neurons discharge periodically during locomotion, but this modulation is eliminated following cerebellar ablation (Arshavsky et al., 1986). Studies of the forelimb area of the paravermis in awake, intact cats performing treadmill locomotion have also reported rhythmic modulation and a wide range of step tuning across the population (Armstrong and Edgley, 1984, 1988; Edgley and Lidierth, 1988). Surprisingly, although most cells have somatosensory climbing fiber receptive fields on the distal part of the forelimb, tuning of complex spikes to step phase is weak or absent (Andersson and Armstrong, 1987; Armstrong et al., 1988). In contrast with studies using the reduced preparation, which documented a reciprocal interaction between Purkinje cells and their nuclear targets (Arshavsky et al., 1986), work in intact cats suggests that the activity peak in the paravermal Purkinje cell population coincides with the peak in the interpositus nucleus (Armstrong and Edgley, 1984).

While a great deal is known about the role of the cerebellum during locomotion, few studies have attempted to record from multiple Purkinje cells in freely-behaving rodents. The present dissertation is concerned with the discharge properties of Purkinje cells in the dorsal vermis of rats during unrestrained locomotion and sleep. Chapter 2 describes our experimental approach. Chapter 3 undertakes a study of step-to-step variability in simple and complex spike patterns during locomotion, as well as the relationship between this variability and movement parameters. Chapter 4 describes Purkinje cell activity in sleeping animals and demonstrates that the parallel and climbing fiber pathways are co-activated by pontocerebellar waves during active sleep.

## 2 Multi-Tetrode Recording in the Cerebellar Cortex of Unrestrained Rats

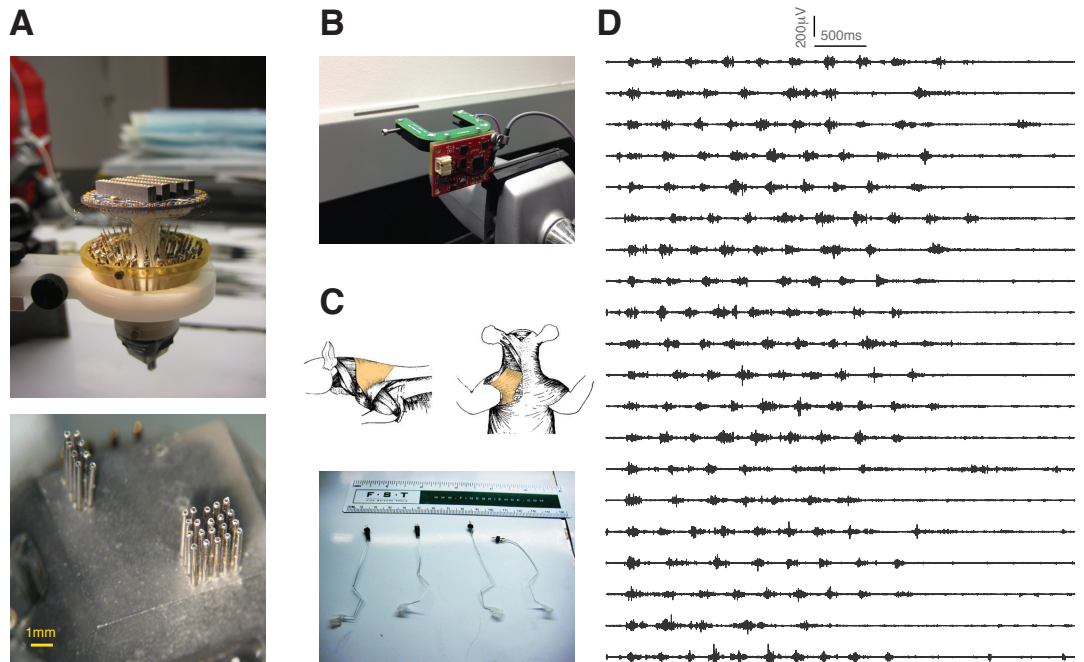
*I insisted on manual instruction, not as an end in itself, or with any idea of turning it to incidental account by actually producing handicrafts, but as providing a good all-round training for hand and eye, and being a practical first step in mastering industrial processes.*

- Walter Gropius, *The New Architecture and the Bauhaus*

While a wide range of experimental approaches to the study of neural activity during behavior are available, the technique of chronic, multi-tetrode recording in rats (Wilson and McNaughton, 1994) offers several key advantages. First, it can be performed in unrestrained animals engaged in natural tasks, such as spatial navigation. Second, it allows stable, long-term measurements from the same neurons, and can therefore be used to study the evolution of activity over learning, over extended sleep sessions, or over a large number of trials in sensorimotor tasks. Third, tetrode arrays allow simultaneous recordings from multiple neurons, and can be used to assess ensemble correlations. Finally, the high temporal resolution of electrophysiology allows the measurement of spike trains from tonically active neurons with firing rates too high to be assessed with calcium indicators. Despite the power and flexibility of the method, multi-tetrode recording has been applied mainly in the hippocampal formation and neocortex. Although the technique has also been used to study other brain structures, such as the striatum (Berke et al., 2004), the ventral tegmental area (Valdes et al., 2015), and the thalamus (Wimmer et al., 2015), few studies have applied it to hindbrain motor regions.

Cerebellar Purkinje cells are a particularly promising target for tetrode recordings, which not only allow unambiguous identification of cell type by the presence of complex spiking, but also a disassociation of parallel and climbing fiber influences on each cell. Microelectrode

Figure 3: Instrumentation. **(A)** Multi-tetrode microdrive array (upper panel) and close-up of custom-machined tip for directing tetrodes to the dorsal vermis, neocortex, and hippocampus (lower panel). **(B)** Headstage-mounted bracket with LEDs for tracking the animal's position and inertial measurement unit for measuring head attitude. **(C)** Acromiotrapezius muscle (upper panel, in orange; Greene, 1968) and bipolar patch EMG electrodes (lower panel). **(D)** Acromiotrapezius EMG data for twenty consecutive laps on a linear track. Each burst corresponds to one step cycle (see Chapter 3).



recordings from these neurons are challenging, however, as the cerebellum moves extensively due to respiration, heartbeat, and — in awake animals — motor behavior. Furthermore, the Purkinje cell layer in mammals is only one cell thick, offering significantly lower cell yields than densely-packed regions like CA1, and the extensive dendritic arbors of Purkinje cells are particularly susceptible to microelectrode damage. Previous experimental attempts with tetrodes in cerebellar cortex have resulted in the isolation of individual Purkinje cells (de Solages et al., 2008; Gao et al., 2012). These recordings, however, relied primarily on large (100 $\mu$ m) commercial quartz tetrodes poorly suited to awake preparations, were typically performed under anesthesia or head fixation, and were not obtained during motor behavior.

We attempted to overcome these challenges by building a multi-tetrode microdrive array for chronic implantation over lobules V and VI of the cerebellar vermis (Figure 3A, 4D). Craniotomy coordinates were 10.5mm to 12mm posterior of bregma, and -1.0mm to 1.0mm lateral of the midline; this location was chosen because the underlying brain was free of large blood vessels, and because it was just anterior enough to allow space for the microdrive assembly. Twenty guide tubes were arranged in a 500 $\mu$ m rectangular lattice in order to sample a large region of cerebellar cortex and to facilitate postmortem identification of tetrode tracks (Figure 4). Each guide tube carried an independently adjustable tetrode attached to a micromanipulator. Tetrodes were fabricated manually, by twisting together four 10 $\mu$ m nichrome wires, fusing the wires with a heat gun, cutting the tetrode tip, and gold plating the contacts. The tracks and terminal locations of the tetrodes were recovered in histology, and were restricted to vermal lobules IV, V, and VI (Figure 4A-C), areas classically associated with the hindlimbs, forelimbs, and head, respectively. We also targeted tetrodes to neocortex and hippocampus to monitor global changes in brain state.



Figure 4: **(A)** Hoechst-stained sagittal section showing cerebellar lobules and cortical layers. Peak of excitation spectrum: 350nm. **(B)** The same section imaged using 480nm excitation. The tetrode track and electrolytic lesion for tetrode 19 are clearly visible. **(C)** Recording locations for all tetrodes. 480nm excitation. **(D)** Design and stereotactic coordinates for custom-built multi-tetrode array.

In order to monitor the locomotor rhythm in freely-moving animals, we performed electromyographic (EMG) recordings from the acromiotrapezius (Figure 3B, above), a muscle offering three distinct advantages. First, it is a large, flat, superficial muscle (Greene, 1968) suitable for targeting with bipolar patch electrodes (Loeb and Gans, 1986; Figure 3B, below), which offer excellent long-term stability in chronic experiments and can be attached to the overlying fascia without traumatizing the muscle. Second, it is located near the posterior boundary of the skull, and can be exposed with minimal modification to the surgical protocol for the implantation of the microdrive array. Third, the acromiotrapezius is known to be rhythmically active during locomotion in cats, with an activity peak late in stance (English, 1978); our own pilot experiments corroborated this observation in rats. In addition to using EMG, we further monitored behavior by measuring the location, pitch, and roll of the head with a ceiling-mounted camera, headstage-mounted LEDs, and an inertial measurement unit (Figure 3B).

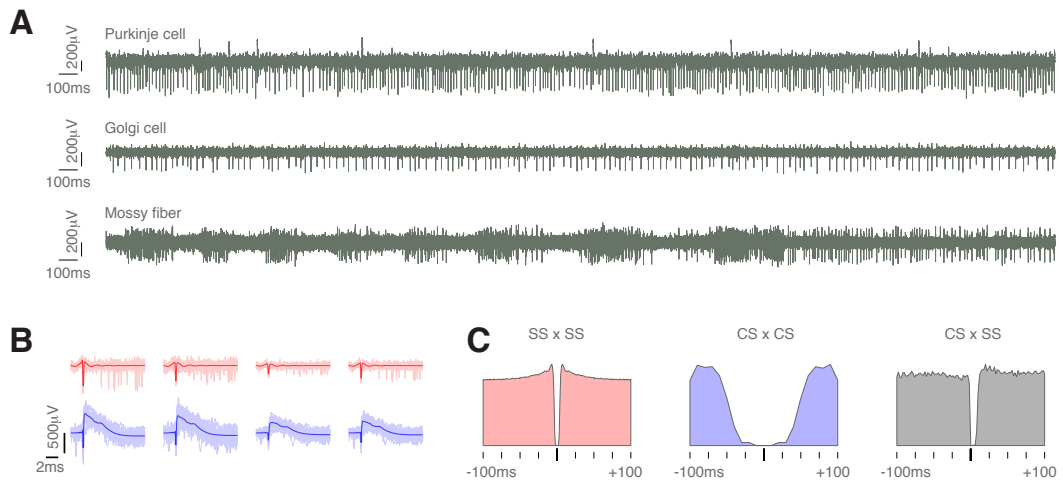
For the surgical implantation, male Long-Evans rats (age 3-5 months) were anesthetized with 2-3% isoflurane and fixed in a stereotaxic frame. The head was shaved, and a single incision was made to expose the skull and anterior portion of the neck. Bipolar patch EMG electrodes fabricated from silicone rubber and multi-stranded steel wire were implanted over the left and right acromiotrapezius muscles. Each corner of the silicone sheet was separately sutured to the fascia, and additional sutures were applied at two kinks in the wire for stress relief. Screws were fixed to the skull for mechanical support. Two craniotomies were made, one overlying the cerebellar vermis, and the other overlying the hippocampus and

neocortex. The dura mater was carefully removed with forceps, and the array of guide tubes was moved to the surface of the brain. The stability of recordings could be improved significantly by pressing gently at this stage. Finally, the guide tubes were sealed with a silicone elastomer, the assembly was fixed to the skull with UV-curable dental cement, the skin was sutured closed, and the animals were recovered from anesthesia and taken to the experimental chamber.

Following several days of recovery from the surgery, we began to carefully move the cerebellar tetrodes and search for single units. Neurons were much more difficult to isolate in cerebellar cortex than in hippocampus or neocortex; on a typical day, most tetrodes exhibited no spiking, and those tetrodes with large spikes yielded one to three single units. Because the adjustment proceeded slowly, in increments of tens of microns per day, our use of arrays of multiple tetrodes parallelized the search process and increased cell yields significantly. When spiking was absent, one of two stereotyped activity patterns was often observed. The first pattern was characterized by a low level of background activity in the spiking band, punctuated by sporadic negative waves of approximately 2ms duration, or fat spikes, which were most easily identified acoustically using a loudspeaker (Gao et al., 2012). These patterns were probably measured in the molecular layer, with the fat spikes corresponding to climbing fiber potentials observed near dendritic current sinks. The second pattern was characterized by a high level of background spiking-band activity, which fluctuated with the animal's movement, but did not produce any single units large enough to be isolated. This pattern persisted as the micromanipulator moved over hundreds of microns, and likely corresponded to activity in the granule cell layer.

Purkinje cells were often encountered immediately after a ventral movement of the tetrode by 20-40 $\mu$ m, but in other cases they appeared gradually, several hours after ad-

Figure 5: Single units recorded in cerebellar cortex. **(A)** Raw data examples for an identified Purkinje cell, a putative Golgi cell, and a putative mossy fiber. The Purkinje cell has a high rate of simple spikes and a low, irregular rate of inverted complex spikes (data are highpass filtered with a 25Hz cutoff to show complex spiking). The putative Golgi cell has a highly regular spike train, a wide spike waveform, and a resting firing rate lower than most Purkinje cells (Edgley and Lidiirth, 1987). The putative mossy fiber shows high-frequency bursts and pauses during an episode of locomotion, and has a narrow, biphasic waveform (Lisberger and Fuchs, 1978). The lower two traces are highpass filtered with a 600Hz cutoff. **(B)** Simple (red) and complex (blue) spike waveforms for the Purkinje cell in **(A)**. **(C)** Simple and complex spike autocorrelations and simple-complex spike crosscorrelation for the Purkinje cell in **(A)**. Complex spikes are followed by a characteristic pause in simple spiking, and many cells then exhibit a rebound in simple spike rates following the pause.



justment. They were distinguished by the conjunction of several features. First, they had narrow spike waveforms (about 250 $\mu$ s) and high resting firing rates, in the range of 30-120 spk/sec (Figure 5A, above). These firing rates fluctuated rapidly during grooming, walking, and somatosensory stimulation of the body and limbs; such modulation was easily detected using a loudspeaker during close observation and manipulation of the animal. Second, complex spikes were apparent as positive, monophasic waves for most fast-spiking units (Figure 5B), and were immediately followed by a brief pause in simple spiking (Figure 5C, right). The amplitude of complex spikes was much more variable across cells than for simple spikes, and tended to be less stable over time. Nonetheless, for around half the identified Purkinje cells, it was possible to maintain stable recordings of simple and complex spikes for the duration of an experimental session, and in a few exceptional cases, for several days. Usually, it was possible to isolate only a single Purkinje cell on one tetrode; when two or three fast-spiking cells could be isolated in the Purkinje cell layer, only one of them had complex spikes large enough for reliable automated discrimination. No obvious behavioral correlates of complex spiking were apparent. Across the array of tetrodes, it was possible to simultaneously measure the activity of several Purkinje cells; although our yields of 2-5 concurrently-recorded cells are lower than those feasible in forebrain regions, they are a significant step beyond previous microelectrode studies of Purkinje cells, which have almost invariably recorded from one cell at a time. Occasionally, other types of units were encountered, and these appeared to fall into two classes. The first class had narrow, positive or biphasic waveforms, a low level of tonic activity, and high frequency bursts (up to 700 spk/sec) that often coincided with animal movement (Figure 5A, bottom). These units were most likely mossy fibers. The other class of unit, encountered rarely, exhibited highly regular spike trains, relatively low resting firing rates, wide spike waveforms, and no

complex spikes (even for high-amplitude examples); units of this type were likely Golgi cells (Figure 5A, middle).

In conclusion, chronic extracellular methods in the cerebellar cortex of rats are challenging, but can yield stable recordings of simple and complex spikes from Purkinje cells during movement. Given the high resting rate of simple spikes and the absence of simple-spike-related calcium signals, such data cannot be obtained using current imaging methods. Furthermore, whole cell and juxtacellular recordings from head-fixed animals are limited by shorter recording durations, and by the strong restrictions they place on animal movement. Thus, the chronic multi-tetrode approach offers a unique and powerful combination of natural behavior, long recording durations, and multiple simultaneously-recorded Purkinje cells, and provides data which cannot be obtained by other means.

### 3 Structured Variability in Purkinje Cell Activity during Locomotion

*If one asks the question, why did Galton and not Quetelet invent the theory of regression and correlation, it is important, as Victor Hiltz has remarked, that in such discussions Galton spoke of the Normal curve as a 'law of deviation'. Thus where Quetelet was thinking of a central tendency, and hence of the mean, Galton, always preoccupied by the exception, was thinking of the tails of the distribution, and of the dispersion.*

*- Ian Hacking, The Taming of Chance*

#### 3.1 Summary

The cerebellum is a prominent vertebrate brain structure that is critically involved in sensorimotor function. During locomotion, cerebellar Purkinje cells are rhythmically active, shaping descending signals and coordinating commands from higher brain areas with the step cycle. However, the variation in this activity across steps has not been studied, and its statistical structure, afferent mechanisms, and relationship to behavior remain unknown. Here, using multi-electrode recordings in freely moving rats, we show that behavioral variables systematically influence the shape of the step-locked firing rate. This effect depends strongly on the phase of the step cycle and reveals a functional clustering of Purkinje cells. Furthermore, we find a pronounced disassociation between patterns of variability driven by the parallel and climbing fibers. These results suggest that Purkinje cell activity not only represents step phase within each cycle, but is also shaped by behavior across steps, facilitating control of movement under dynamic conditions.

#### 3.2 Introduction

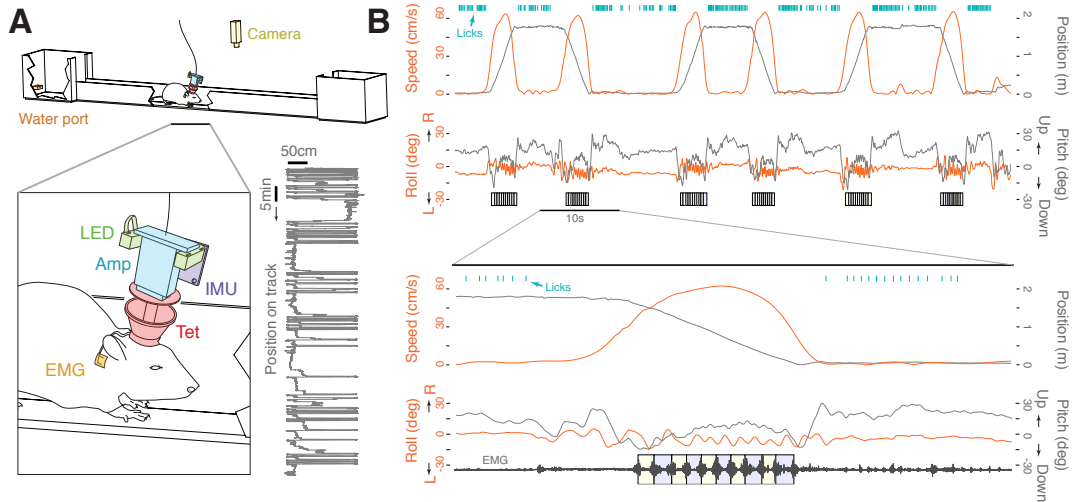
Trial-to-trial variability is a widespread and fundamental feature of neural activity, evident from the periphery through higher brain areas. Responses to sensory stimuli vary over

repeated presentations, and this variability is modulated by stimulus onset (Churchland et al., 2010; Monier et al., 2003), depends strongly on network architecture (Litwin-Kumar and Doiron, 2012), and is altered by successive stages of sensory processing (Kara et al., 2000). Furthermore, trial-to-trial correlations between neurons influence the accuracy of neural codes (Averbeck et al., 2006; Moreno-Bote et al., 2014), and are highly dependent on global changes in brain state (Ecker et al., 2014). During the preparation and execution of movement, neural activity often varies considerably across repetitions, even when the movement is highly stereotyped. Such variability is thought to impose critical constraints on motor performance (Shenoy et al., 2013; Todorov and Jordan, 2002), the capacity of motor codes (Averbeck and Lee, 2003; Lee et al., 1998; Maynard et al., 1999), and learning (Chaisanguanthum et al., 2014; Mandelblat-Cerf et al., 2009).

Several features make locomotion a powerful framework for studying neural variability in motor systems. First, locomotion is an ethologically relevant, nearly universal characteristic of animal life. Many aspects of legged overground movement are remarkably consistent across a wide range of species, from stick insects to humans (Orlovsky et al., 1999; Shik and Orlovsky, 1976), and the insights obtained from its study will likely generalize beyond the model organism chosen. Second, locomotion and other periodic behaviors are paradigmatic cases of motor repetition, with centrally generated rhythms shaped by modulatory influences. Third, studying locomotion eliminates the need for delays between experimental trials, allowing efficient acquisition of data from a large number of cycles and improving the statistical detection of patterns.

The cerebellum plays a critical role in the coordination of locomotion (Armstrong, 1988; Arshavsky et al., 1986; Shik and Orlovsky, 1976), and damage to the cerebellar vermis severely impairs the control of limbs and posture in animal models and in human patients

Figure 6: Experimental setup and behavior on the linear track. **(A)** Rats were trained to walk for water reward on a 1.8m long track. Animal position was measured using an overhead camera and an LED bracket fixed to the headstage (LED). Head pitch and roll were monitored using an inertial measurement unit (IMU), and the stepping rhythm was detected using an electromyogram from the acromiotrapezius (EMG). Purkinje cell activity was recorded using a multi-tetrode array (TET) and headstage-mounted preamplifier (AMP). Behavior in a typical session is shown in the lower right: the animal's position (x-axis) is plotted as a function of time (y-axis). **(B)** Above: animal speed (orange) and position (gray) over the course of six laps, along with head roll (orange), head pitch (gray), lick times (teal), and step segmentation (yellow and blue rectangles). Below: a ten-second segment of the same data showing a single track traversal, including the raw EMG trace.



(Dow and Moruzzi, 1958; Martino et al., 2014; Morton and Bastian, 2004). Furthermore, mouse mutant lines with cell-type-specific abnormalities in the cerebellar cortex exhibit locomotor deficits in speed, accuracy, consistency, and multi-joint coordination (Vinueza Veloz et al., 2014). During stepping, pathways from the spinal cord carry proprioceptive, cutaneous, and rhythmogenic signals to the cerebellar cortex (Arshavsky et al., 1986; Bosco and Poppele, 2001; Oscarsson, 1965). Mossy fibers related to the forelimbs, hindlimbs, and head have different distributions over cerebellar lobules but largely overlap (Adrian, 1943; Anderson, 1943; Dow and Moruzzi, 1958; Matsushita and Hosoya, 1979; Snyder et al., 1978; Tolbert and Gutting, 1997), and vestibular pathways terminate in the same areas (Barmack et al., 1992; Barmack et al., 1993; Denoth et al., 1979; Jensen, 1985; Kotchabhakdi and Walberg, 1978; Manzoni et al., 1999; Matsushita and Wang, 1987; Precht et al., 1977). Signals from these pathways are relayed through the parallel fibers to Purkinje cells in the vermal and intermediate cortex, which discharge periodically during stepping (Armstrong and Edgley, 1984, 1988; Edgley and Lidieth, 1988; Orlovsky, 1972; Udo et al., 1981) and impose their rhythm on routes descending back to the spinal cord (Arshavsky et al., 1986). This rhythmic discharge provides direct signals to the spinal limb controllers, and also gates motor commands from higher brain centers, ensuring that these commands are coordinated with the ongoing locomotor pattern (Orlovsky et al., 1999).

Although the cerebellar contribution to the control of locomotion has been studied extensively, a number of experimental challenges remain. Previous studies have used decerebrate (Arshavsky et al., 1986; Orlovsky, 1972; Udo et al., 1981) and awake (Armstrong and Edgley, 1984, 1988; Edgley and Lidieth, 1988) cats restricted on a treadmill, but none have examined step-locked simple and complex spikes in freely behaving rodents. Furthermore, treadmill studies of constant-speed stepping have dominated the study of cerebellar

Figure 7: Purkinje cell activity during the initiation and termination of movement and during licking. (Continued on the following page.)

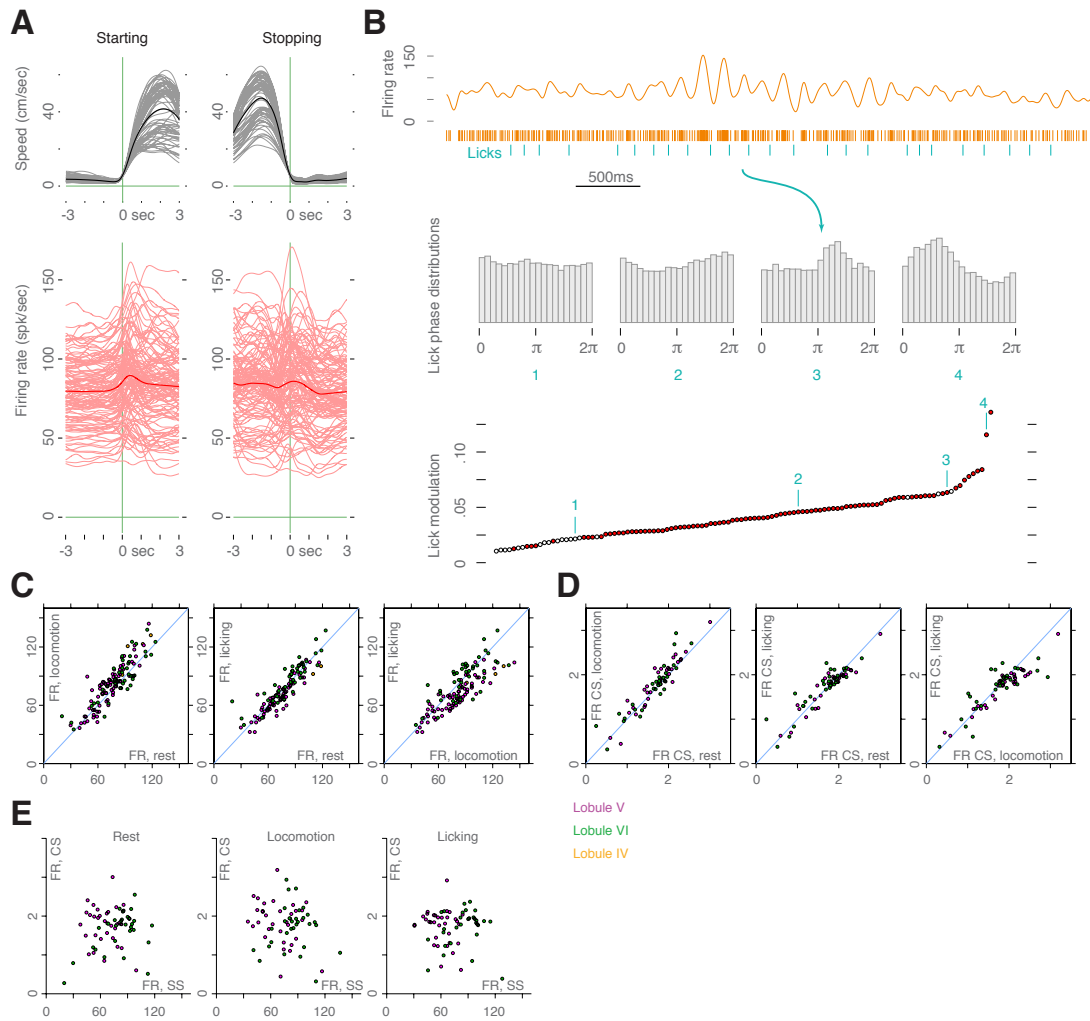


Figure 7: **(A)** Above: animal speed centered on the beginning (left) and end (right) of laps. Each gray curve is the average speed for a single dataset, and the black curves are the averages. Below: Purkinje cell firing rates centered on the beginning and end of laps. Each light red curve is a single cell, and the bold red lines are averages. Most cells exhibit a large phasic increase in firing rate at movement onset and a smaller tonic increase during locomotion. Many also show phasic increases or decreases in firing rate during stopping. Spike trains were smoothed with a 200ms Gaussian kernel. **(B)** Many Purkinje cells discharge rhythmically during licking. Top: example spike raster for a single licking bout. Middle: lick phase histograms for four example Purkinje cells. The three cells on the right are significantly tuned to lick phase. Bottom: distribution of lick tuning values (Kuiper’s statistic) for all Purkinje cells. Significantly tuned cells are red. **(C)** State-dependent firing rates for pairs of states. For most cells, firing rates are elevated during locomotion, relative to rest and licking. **(D)** State-dependent complex spike rates for pairs of states. Rates were higher during locomotion than rest and licking. **(E)** State-dependent complex versus simple spike firing rates. Simple and complex spike rates are not correlated for any state.

activity, but are limited in their ability to reveal the neuronal dynamics that occur in freely moving animals that spontaneously initiate, maintain, and terminate locomotion. Several studies have imaged calcium transients in Purkinje cell ensembles, revealing olivo-cerebellar interactions during locomotion (De Gruijl et al., 2014; Flusberg et al., 2008; Ghosh et al., 2011; Hoogland et al., 2015; Ozden et al., 2012). These transients, however, reflect complex spikes, which constitute only a small fraction of the spiking output. Few simultaneous recordings of simple spikes from multiple Purkinje cells have been made during locomotion (Smith, 1995), and correlations between pairs of neurons across steps have not been studied. Finally, Purkinje cell activity has been reported to vary extensively across steps (Armstrong and Edgley, 1984), but there has been no systematic study of this variation and its relationship to behavior, though some evidence suggests that animal speed can influence activity averaged over many steps (Armstrong and Edgley, 1988).

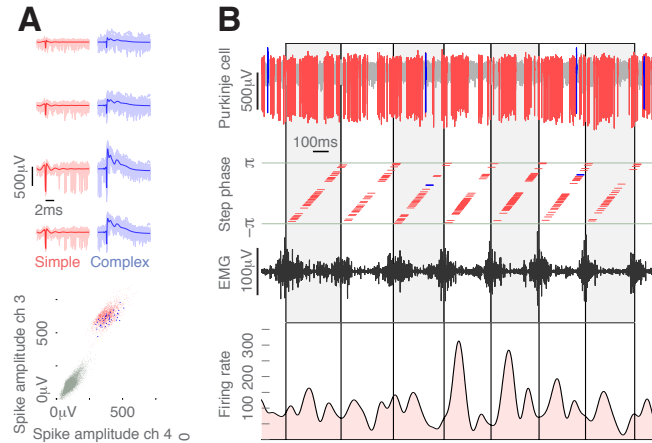
Here, we use chronically implanted multi-tetrode arrays in conjunction with electromyography and behavioral measurements in freely moving rats to address several open questions. First, is the step-locked firing pattern for a Purkinje cell highly stereotyped, or does it change

extensively across steps? Furthermore, if this pattern is flexible, what are its major modes of variation? Second, how is neuronal variability related to behavior? Correlations between neuronal activity and behavioral factors would suggest that step-to-step variation plays a functional role in motor control, while the absence of correlations might indicate that such variation is noise. In addition, if such correlations are present, do they influence only the mean firing rate within a step cycle, or does interaction between behavior and spiking occur on a finer time scale through step-phase-dependent effects? Third, is the activity of multiple Purkinje cells correlated across steps? Uncorrelated activity would suggest that variation reflects intrinsic noise at the level of individual neurons, while pairwise correlations would be consistent with coordinated inputs. Fourth, how is Purkinje cell output shaped across steps by its two afferent systems (the parallel and climbing fibers)? The contributions of these two pathways can be distinguished using extracellular recording: the parallel fibers control the rate of simple spikes, while the climbing fibers produce complex spikes (Eccles et al., 1966). One possibility is that both pathways use an analog rate code for sensorimotor variables both within steps (representing step phase) and across steps (representing behavioral factors such as speed). Alternatively, the two pathways might encode distinct features using qualitatively different coding schemes.

### **3.3 Results**

Using chronically implanted multi-tetrode arrays, we recorded spiking activity from 120 Purkinje cells in the medial cerebellar vermis of freely behaving rats ( $n=3$ ; Figure 6A). Most cells were located in lobule V ( $n=74$ ) and VI ( $n=42$ ), with a small number in lobule IV ( $n=4$ ). All recorded neurons were identified as Purkinje cells by the presence of complex spiking (Eccles et al., 1966), and in many of these cells ( $n=65$ ) it was possible to reliably

Figure 8: Tetraode recording from a Purkinje cell during a traversal across the track. **(A)** Simple (red) and complex spike (blue) waveforms for all four channels, as well as spike amplitudes on a pair of channels, are shown. **(B)** Raw data from a single tetraode channel, along with step phases at spike times and EMG trace (black). The EMG peaks correspond to a step phase of  $\pi$ . The firing rate of the Purkinje cell is shown in the bottom panel. Within each step cycle, the firing rate changes with step phase, but the shape and magnitude of these changes vary extensively across steps.



distinguish between simple and complex spikes throughout the session (Figure 8A). The animals were trained to walk freely on a linear track for water reward at ports positioned at the ends of the track, while we recorded head location, head attitude, an EMG of acromio-trapezius activity, and the timing of licks at the water ports (Figure 6B). For most cells, firing rates were elevated during locomotion, relative to inactivity and licking (Figure 7C,  $p < 10^{-7}$  and  $p < 10^{-6}$ , respectively, paired t-tests), and complex spikes also exhibited rate increases for the same states (Figure 7D,  $p = .0011$  and  $p = .015$ , paired t-tests). Phasic increases in firing occurred at the onset of locomotion, and phasic increases or decreases were common during movement termination (Figure 7A). Lick times were recorded for 114 cells, and 101 of these were significantly modulated by licking (Figure 7B, Kuiper's test, false discovery rate set at  $q = .05$ ).

All cells discharged rhythmically during locomotion (Figure 8B, 9A, B);  $q = .05$ , Kuiper's

Figure 9: Purkinje cell activity is rhythmically modulated during locomotion, but highly variable across steps. (Continued on the following page.)

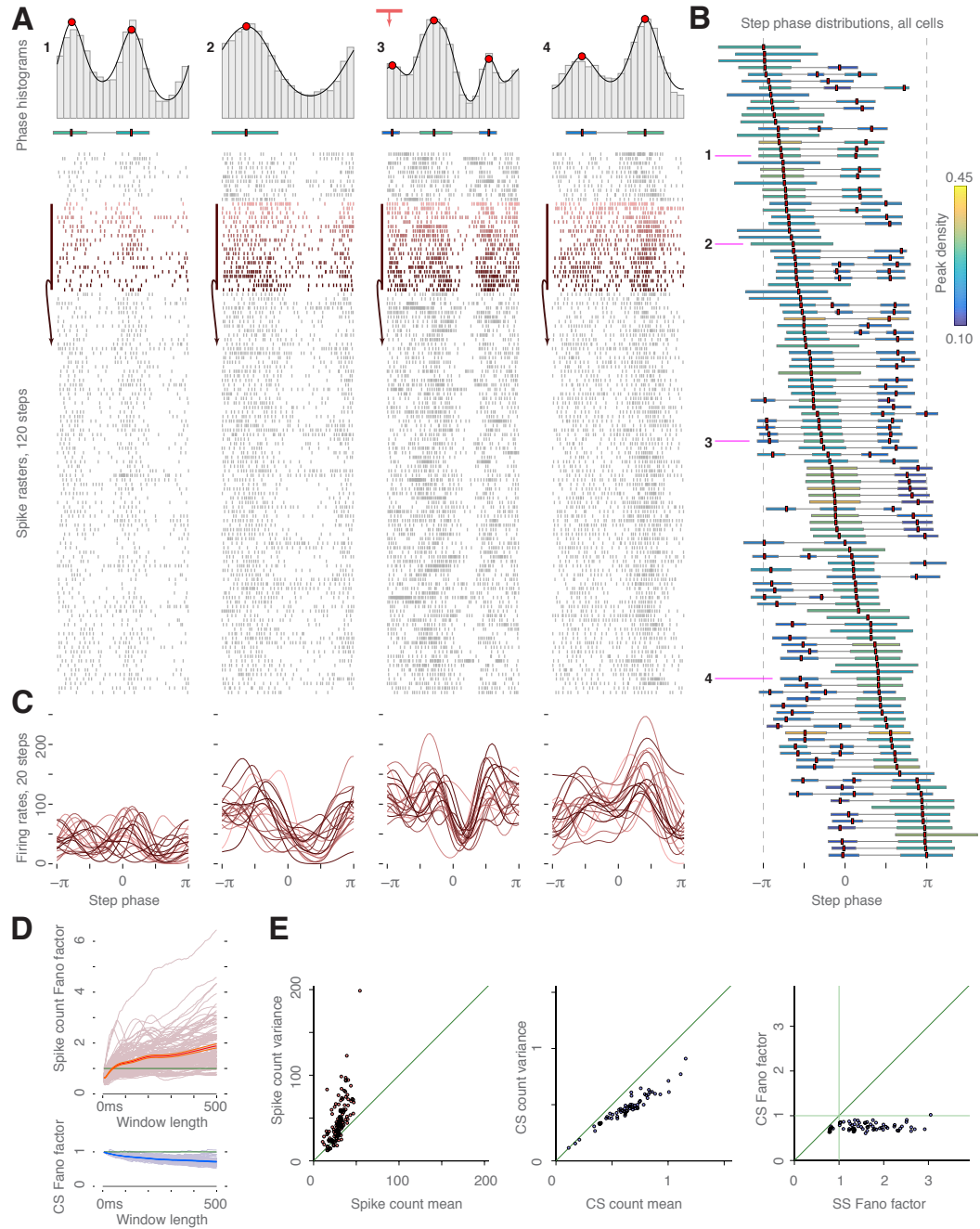


Figure 9: **(A)** Above, histograms of the step phase at spike times and density fits for four neurons. The example cell from figure 8 is marked with a red arrow. Below, step-locked spike rasters for the first 120 steps from each dataset. Darker colors represent later cycles. **(B)** All recorded Purkinje cells were significantly tuned to the stepping rhythm, but the number, location, and height of the modes were diverse. Each red marker corresponds to one mode, and the horizontal extent of each bar corresponds to half the distance between the mode and the nearest trough. The scale bar shows the height of the density peaks, encoded as pseudocolor hue. **(C)** Step-locked firing curves for twenty consecutive steps, colored as in **(A)**. These curves exhibit a high degree of variability, which is not evident in the averaged data. **(D)** Variance-to-mean ratios (Fano factors) for step-locked spike counts (above) and complex spikes (below). Each curve represents the Fano factor for a single cell, as a function of the length of the window starting at the EMG peak. Bold lines represent the averages across cells,  $\pm$  SEM. The solid green lines show the Fano factor expected for a Poisson process, which is identically one. **(E)** From left to right: spike count variance versus mean, complex spike variance versus mean, and complex versus simple spike Fano factor for a 350ms window. These data indicate that simple spikes are significantly over-dispersed relative to a Poisson process, while complex spikes are under-dispersed.

test), consistent with previous studies of paravermal lobule V in awake cats on a treadmill (Armstrong and Edgley, 1984, 1988; Edgley and Lidieth, 1988). Cells exhibited one ( $n=26$ ), two ( $n=69$ ), or three ( $n=25$ ) peaks in the step cycle, and the location of these peaks was widely dispersed across cells (Figure 9B). However, although the average activity of each cell exhibited clear tuning to step phase, an inspection of spiking patterns across individual steps revealed a high degree of variability. The firing rate of the Purkinje cell in Figure 8, for instance, shows large fluctuations within each step cycle, but even more striking are the changes in its amplitude and shape across steps. This extensive step-to-step variability was typically observable in the step-locked spike rasters (Figure 9A, lower panel) and firing rate curves (Figure 9C).

In order to quantify this variability, we computed the variance-to-mean ratio, or Fano factor, for the spike counts within a window starting at the EMG peak for each step cycle (Figure 9D, above). For a Poisson process, the count variance equals the count mean, and the Fano factor is one. By contrast, Purkinje cell spike counts typically had higher variances than means (Figure 9E, left panel), with a mean Fano Factor of 1.58 for a window duration

of 350ms. These values indicate that spiking is more variable than expected for a Poisson process, and more variable than previously reported for macaque neocortical neurons during visually-guided reaching (e.g., supplementary motor area (Averbeck and Lee, 2003; Mandelblat-Cerf et al., 2009), motor cortex (Mandelblat-Cerf et al., 2009), premotor cortex (Churchland et al., 2010; Churchland et al., 2006), and the parietal reach region (Churchland et al., 2010)). Interestingly, we observed a strong disassociation between patterns of variability for simple spikes, which were over-dispersed relative to a Poisson process, and for complex spikes, which were under-dispersed (Figure 9D, below, 9E, center and right).

If firing patterns differ across steps, what are the major modes of variation? In order to address this question, we performed principal component analysis on the step-locked firing rates for each cell. This produced an effective reduction of the data, with the first three components accounting for an average of 75% of the variance (Figure 10C, left). Sorting cycles by principal component scores (Figure 10A) or visualizing the effects of the coefficients as perturbations of the mean firing rate curve (Figure 10B) revealed several common patterns: bias (an additive shift in the curve with little change in its shape), amplitude (multiplicative scaling of the curve), and phase (a horizontal shift of the curve forward or backward in time). These same three patterns have been independently identified in kinematic data from humans during locomotion (Ramsay and Silverman, 2005). While many cells had components that directly reflected one of these modes, more complex patterns were observed, as well. For instance, some cells with multiple peaks exhibited components that shifted the firing rate around one of the peaks, while imposing little change on the rest of the curve (e.g., component 1 for the cell marked with red arrow in Figure 10B, corresponding to the neuron from Figure 8).

To quantify the extent to which a component represented a change in bias, amplitude,

Figure 10: Patterns of step-to-step variability. (Continued on the following page.)

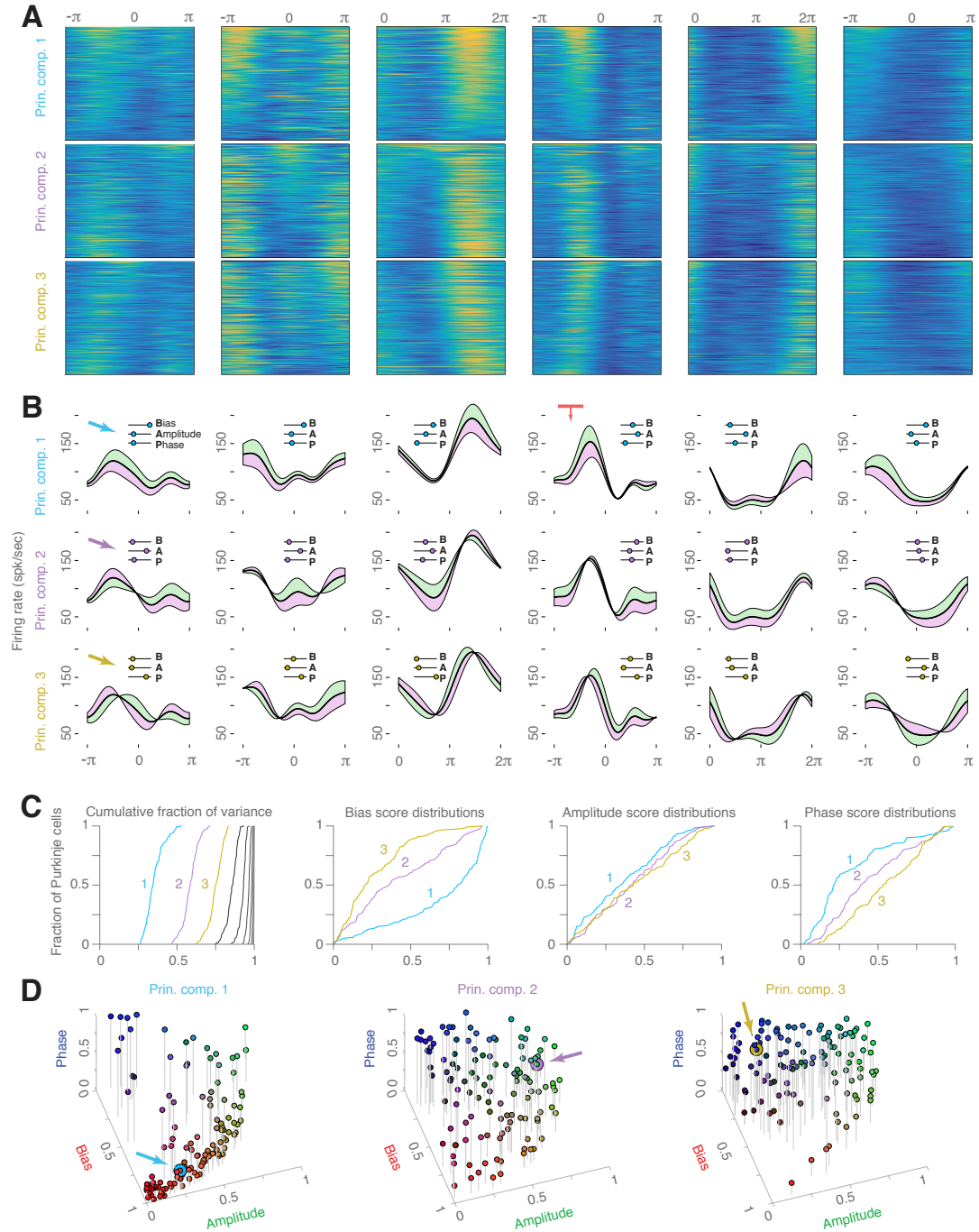
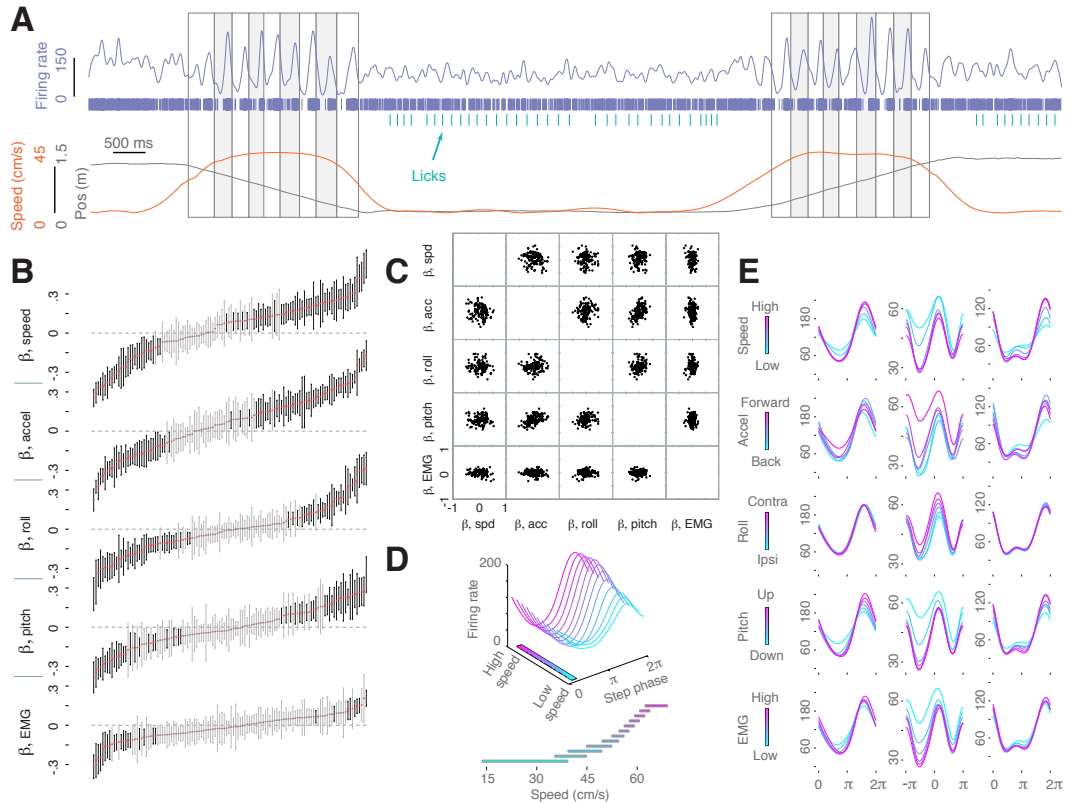


Figure 10: **(A)** Firing rates on all step cycles for six Purkinje cells (columns), ordered by scores for the first three principal components. **(B)** Mean firing rate curves (black) for the cells in **(A)**. Each row shows the effect of adding or subtracting one of the first three principal components for each cell. For a mean firing rate curve  $f(\theta)$  and a principal component coefficient vector  $w(\theta)$ , the green curve shows  $f(\theta) + cw(\theta)$ , and the magenta curve shows  $f(\theta) - cw(\theta)$ , where  $c = 100$  is a constant. In many cases, the components impose a shift in bias, amplitude, or phase. In each panel, the three inset scales show (1) bias score,  $S_{bias}$ , (2) amplitude score,  $S_{amp}$ , and (3) phase score,  $S_{phase}$ . The example cell from figures 7 and 8 (fourth column) is marked with a red arrow. **(C)** Distribution of curve properties across the Purkinje cell population. The left panel shows the cumulative fraction of curve variance due to the first (blue), second (lavender), third (yellow), and fourth through tenth (gray) principal components. The three panels on the right show the distribution of bias, amplitude, and phase scores for each of the first three components. **(D)** Joint distribution of bias, amplitude, and phase scores. In the left panel, the location and RGB value of each point represent  $(S_{bias}, S_{amp}, S_{phase})$  for the first principal component of a single Purkinje cell. For example, the cell marked with the blue arrow is the cell in the first column in **(B)**, and the location of this point corresponds to the bias, amplitude, and phase values on the inset scale in the first row and first column of **(B)**. This cell exhibits a high bias value, but low amplitude and phase values. Similarly, the center and right panels show  $(S_{bias}, S_{amp}, S_{phase})$  for the second and third components, respectively. For many cells, the first component (left panel) is close to a pure bias shift:  $(S_{bias}, S_{amp}, S_{phase}) \approx (1, 0, 0)$  (red points). By contrast, the third component (right panel) often reflects a phase shift:  $(S_{bias}, S_{amp}, S_{phase}) \approx (0, 0, 1)$  (blue points).

or phase, we computed three scores corresponding to these patterns:  $S_{bias}$ ,  $S_{amp}$ , and  $S_{phase}$  (see methods section). Across the sample of Purkinje cells, the first principal component had much higher bias scores than the second ( $p < 10^{-9}$ , Kolmogorov-Smirnov test) and third ( $p < 10^{-23}$ ) components (Figure 10C), and the second component had higher bias scores than the third ( $p < 10^{-4}$ ), indicating that differences across steps were due largely to shifts in the mean firing rate. By contrast, the phase shift scores were much lower for the first principal component than for the second ( $p < 10^{-6}$ ) and third ( $p < 10^{-11}$ ), and for the second than the third ( $p = .0023$ ). Furthermore, three-dimensional scatterplots revealed an aggregation of neurons around a pure bias shift for the first component, and around a pure phase shift for the third component (Figure 10D).

Are these step-to-step fluctuations in neuronal spiking related to behavior? Examination of the spiking activity of individual neurons over several laps often suggested systematic

Figure 11: Behavior modulates step-to-step variability. **(A)** Spike train and firing rate for a Purkinje cell over two laps, along with the animal's position and speed, and step and lick times. regression of step-locked average firing rates against step-averaged behavioral variables. **(B)** Regression coefficients and 95% confidence intervals for all cells, sorted by coefficient value. Coefficients significantly different from zero are shown in black, with the coefficients not reaching significance in gray. All variables are Z-scores. Most Purkinje cells are modulated by speed, acceleration, or head posture across steps. **(C)** Scatterplots of regression coefficient pairs. Each subplot corresponds to a pair of behavioral variables, and each point represents the pair of regression coefficients for a single cell. **(D)** Above: wireframe plot showing the dependence of firing rate on animal speed for the cell in **(A)**. Each curve is the average firing rate for steps on which the animal's speed falls within the specified slicing interval. Note the smooth transition from a low-amplitude to high-amplitude curve with increasing speed. Below: slicing intervals used in upper panel. Twelve slicing intervals are used, with 50% overlap. **(E)** Speed-, acceleration-, roll-, pitch-, and EMG-dependent firing rates for three example cells. Six slicing intervals are used, with 50% overlap. The neuron from **(A)** is shown in the left column.



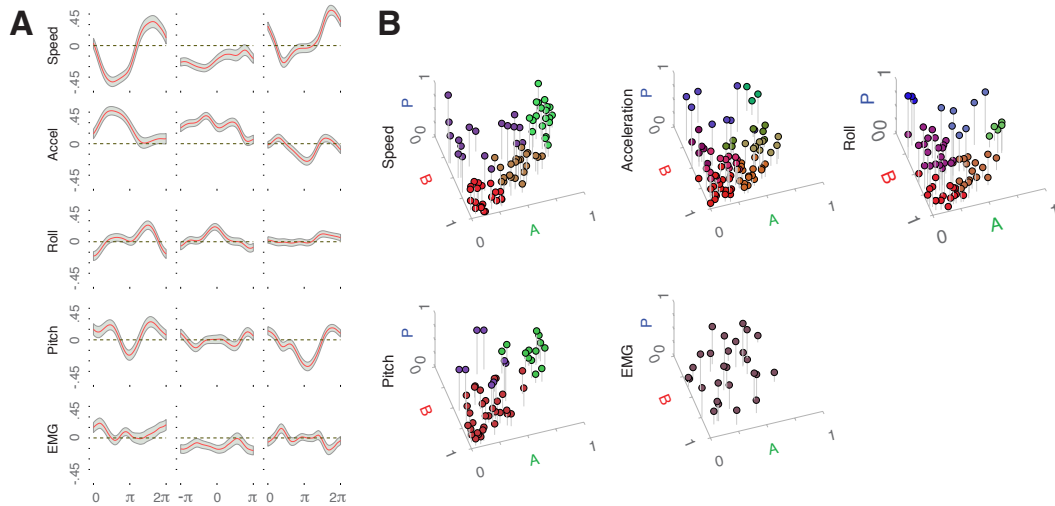
changes in step-locked firing rates with behavioral variables, such as speed (Figure 11A). In order to characterize this further, we first measured the animals' average head speed, acceleration, roll, pitch, and EMG amplitude within each step and examined their relationship to the firing rates. For each neuron and behavioral variable, we divided the steps into intervals according to the value of the variable and averaged the firing rate curves within each interval (see methods section). This often produced a sequence of curves that varied smoothly and systematically as the behavioral parameters changed (Figure 11D, E). In order to quantify the effects of behavior on neuronal activity, we estimated a linear model for each Purkinje cell, with speed, acceleration, roll, pitch, and EMG amplitude as independent variables and the mean firing rate on each cycle as the dependent variable. Speed, acceleration, and head attitude had significant effects for many cells. Out of 120 total Purkinje cells, 81 were modulated by speed, 84 by acceleration, 70 by roll, and 54 by pitch (Figure 11B). By contrast, only 27 neurons were significantly modulated by EMG amplitude. For each independent variable, both positive and negative regression coefficients were observed, but most significant values were positive for speed ( $p = .014$ , binomial test). An examination of coefficients for pairs of variables failed to reveal any clustering of Purkinje cell tuning properties: instead, a broad distribution of values was observed (Figure 11C).

If behavior is correlated with Purkinje cell activity, what is the structure of its relationship to the step-phase-dependent firing rate? This question is central, for two reasons. First, cycle-to-cycle variability is not restricted to shifts in mean firing rate, but can express a variety of patterns, as indicated by the analysis of principal component coefficients (Figure 10). Second, the behavioral variables particularly roll, pitch, and EMG amplitude can fluctuate on a faster time scale than that of a single step cycle (Figure 6B). In order to address this question, we estimated regression curves parameterized by step phase for each cell and

behavioral variable. These curves capture how a given behavioral variable modulates the shape of the step-locked firing rate for each cell. For many cells, the relationship between behavior and neural activity varied in magnitude, and in some cases in sign, according to the phase of the step cycle (Figure 12A). For example, the neuron on the left in Figure 11E shows a decrease with speed during the first half of the step cycle, but an increase with speed during the second half. Consequently, this neuron’s speed regression curve has a shape similar to its average firing rate curve (Figure 12A, left column), and imposes a strong amplitude shift. To further quantify the patterns of this behavioral modulation, we computed bias, amplitude, and phase scores for these curves (see Supplemental Experimental Procedures). Three-dimensional scatterplots of scores ( $S_{bias}$ ,  $S_{amp}$ , and  $S_{phase}$ ) for the regression curves revealed large differences between behavioral variables, as well as the presence of clusters (Figure 12B). We performed a hierarchical cluster analysis on the ( $S_{bias}$ ,  $S_{amp}$ ,  $S_{phase}$ ) observations for cells with significant tuning to each variable, and this analysis revealed several key features. First, all variables except EMG amplitude exhibited a large aggregation of cells around a pure bias shift. Second, speed and pitch exhibited clusters near a pure amplitude shift. Third, roll and acceleration exhibited clusters near a pure phase shift. These results demonstrate a functional segregation in Purkinje cell properties that is not observed after averaging behavior and firing rates within each step cycle.

In many sessions, it was possible to record simultaneously from multiple Purkinje cells, and step-averaged firing rates for pairs often appeared to covary across steps (Figure 13A). Such covariation may result in part from similar tuning to measured behavioral variables, so we first removed the effects of these factors using the regression models and then examined correlations between the residuals. Scatterplots of the residual firing rates for pairs recorded on distinct tetrodes revealed clear associations in many cases (Figure 13B, above), and 40

Figure 12: Behavioral modulation depends strongly on step phase. **(A)** Phase-dependent regression curves. Bands show 95% confidence intervals. Behavior has a strong, phase-dependent effect on firing rates for many cells, which varies across different behavioral variables. **(B)** Bias, amplitude, and phase analysis of regression curves reveals functional clustering of Purkinje cells. For each behavioral variable, the 3D scatterplot shows  $(S_{bias}, S_{amp}, S_{phase})$  values of the regression curves for cells significantly modulated by that variable. Points are colored using RGB values of the cluster averages of  $(S_{bias}, S_{amp}, S_{phase})$ . Note a concentration of points around  $(S_{bias}, S_{amp}, S_{phase}) = (1, 0, 0)$  (bias shifts) for all behavioral variables except EMG amplitude, around  $(S_{bias}, S_{amp}, S_{phase}) = (0, 1, 0)$  (amplitude shifts) for speed and pitch, and around  $(S_{bias}, S_{amp}, S_{phase}) = (0, 0, 1)$  (phase shifts) for acceleration and roll.



out of 89 pairs were significantly correlated (Figure 13B, below;  $q = .05$ , partial rank correlation), with both positive and negative correlations observed. Further analysis of the residuals and the rank-transformed variables indicated that the correlations were unlikely to be due to nonlinear interactions between measured behavioral variables and firing rates. These correlations suggest that step-to-step variability is not independent, intrinsic noise at the level of individual Purkinje cells, but is rather driven by coordinated inputs. The relative spatial location of recorded cells did not influence correlations: no significant differences were observed between ipsilateral and contralateral pairs ( $p = .27$ , two-sample t-test), between cells in the same lobule and in different lobules ( $p = .35$ , two-sample t-test), or between cells at different mediolateral or rostrocaudal distances ( $p = .95, .92$ , respectively, one-way ANOVA) (Figure 13C).

Because the climbing fiber system plays an essential role in motor performance and learning, we examined the relationship between complex spikes, which are driven by this pathway, and step phase, speed, acceleration, head posture, and EMG. In contrast to simple spikes, which were strongly modulated by the stepping rhythm for all Purkinje cells, complex spikes were modulated in a minority of neurons (12/65;  $q = .05$ , Kuiper's test; Figure 14A, B). The depth of modulation was larger for simple than complex spikes ( $p < 10^{-9}$ , paired t-test), though high values were occasionally observed for complex spikes (Figure 14B, left). Most of these observations, however, were from datasets with relatively few steps (Figure 14B, right), and did not achieve statistical significance, suggesting that some large deviations from uniformity might have been artifacts of small sample size. Furthermore, the estimation of linear models for step-locked spike counts failed to reveal effects of speed, acceleration, roll, pitch, and EMG amplitude: no regression coefficients differed significantly from zero ( $q = .05$ , Figure 14C). Thus, our data suggest that while simple spikes are strongly related

Figure 13: Step-to-step variability is correlated across Purkinje cells. **(A)** Stepping sequences on four consecutive laps, along with spike trains and firing rates for a pair of simultaneously-recorded neurons (orange and teal). The step-averaged firing rates, shown as dots, often suggested coordinated changes between pairs. **(B)** Above: a scatterplot of residual firing rates for the pair of cells in **(A)** reveals that the step-averaged firing rates were correlated after removing the effects of behavioral factors. These correlations were not due to nonlinear interactions between measured behavioral variables and firing rates. Below: the partial rank correlations (Spearman's  $\rho$  for the regression residuals) between firing rates for pairs of cells (z-scores) are shown with 95% confidence intervals (above). Many pairs are significantly correlated ( $q = .05$ , bold), both positively and negatively. **(C)** Pairwise correlations do not depend on the relative anatomical location of the recorded cells. Panels show the distribution of correlation values for pairs on the same and opposite sides of the brain, in the same or different lobules, and as a function of mediolateral and rostrocaudal separation. Correlation values significantly different from zero are plotted in red.

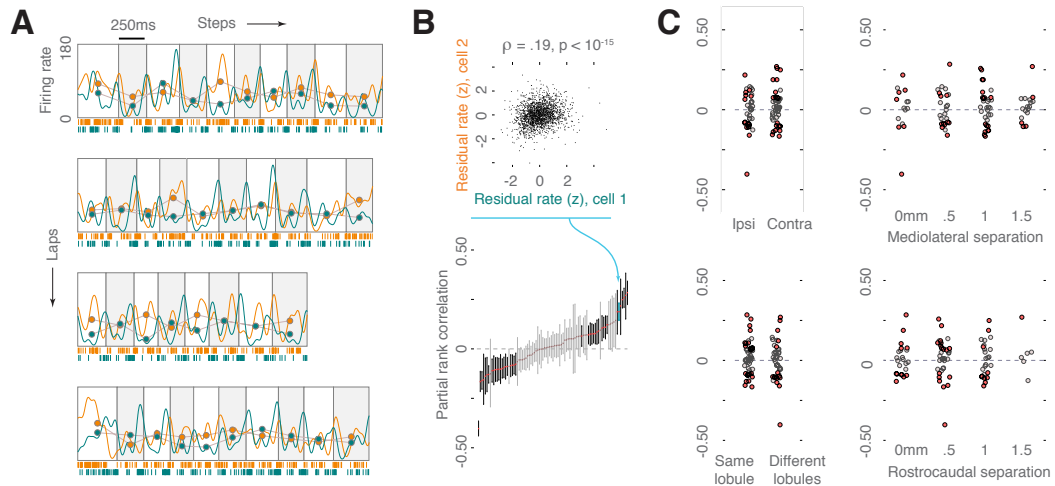
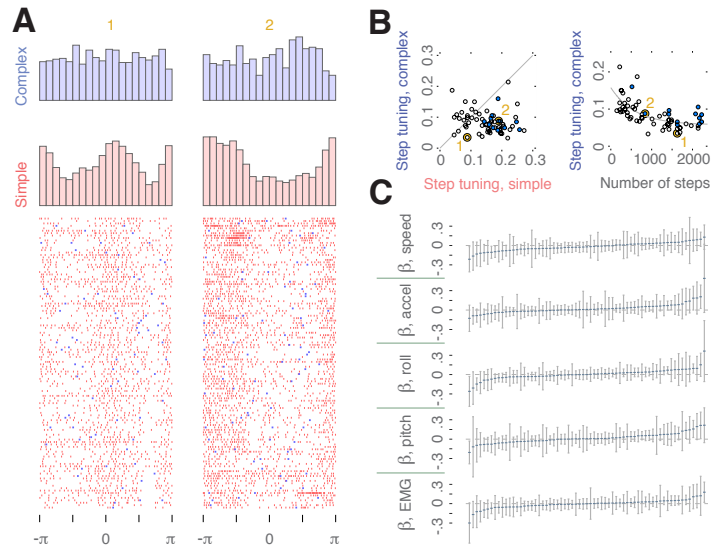


Figure 14: Complex spikes show modest tuning to step phase, but are not related to behavioral variables across steps. **(A)** Simple spike (red) and complex spike (blue) step phase histograms for the two example Purkinje cells highlighted in orange, along with the spike rasters for the first 120 steps. Cell 2 showed statistically significant complex spike tuning. **(B)** Left: step tuning strength (Kuiper’s statistic; see Methods) for simple and complex spikes. Cells with significant complex spike tuning are plotted in blue. Simple spike tuning was significant for all recorded cells. Right: complex spike step tuning strength against the number of steps in the dataset. Some of the largest values of step tuning strength likely result from a small number of observed step cycles. **(C)** Linear model coefficients for behavioral predictors of complex spikes, with 95% confidence intervals. Complex spikes are not significantly modulated by speed, acceleration, head posture, or EMG amplitude for any cells. These results suggest that the parallel and climbing fiber systems convey distinct types of information during locomotion.



to locomotor behavior within steps (through step phase) and across steps (through speed, acceleration, and head posture), complex spikes show only modest tuning to step phase, and no tuning to behavioral variables across steps.

Although the mossy fiber pathways into cerebellar lobule V and into lobule VI overlap extensively, they differ in their density, anatomical origin, and function. For instance, proprioceptive and cutaneous pathways from the forelimbs terminate more extensively in lobule V, whereas inputs from the head and neck are more prominent in lobule VI (Adrian, 1943; Anderson, 1943; Barmack et al., 1992; Barmack et al., 1993; Dow and Moruzzi, 1958;

Kotchabhakdi and Walberg, 1978; Matsushita and Hosoya, 1979; Snyder et al., 1978; Tolbert and Gutting, 1997). We therefore explored potential differences between our samples of lobule V and lobule VI Purkinje cells. Although cells in both regions were tuned to the stepping rhythm and exhibited speed-, acceleration-, and head posture-related variation across steps, several differences between lobules emerged. In lobule VI, mean firing rates were higher (Figure 15B,  $p < 10^{-4}$ ), and there was a stronger relationship between head posture and step-locked activity ( $p = .012$ ), while lobule V cells were more strongly modulated by acceleration ( $p = .0011$ ). Although we observed lobular differences in the distributions of several features, these distributions were largely overlapping, and did not result in a clear separation of lobule V and VI neurons (Figure 15C). Furthermore, a higher fraction of cells had multiple peaks in the step cycle for lobule V than lobule VI (Figure 15A; 91% vs 55%,  $p < 10^{-4}$ , Fisher’s exact test). These differences are consistent with a functional segregation in the vermis during locomotion, with lobule V playing a greater role in limb control and lobule VI acting to maintain postural stability of the head.

### 3.4 Discussion

The data obtained and analyzed here represent, to our knowledge, the first recordings of simple and complex spikes from cerebellar Purkinje cells in freely moving rodents during stepping, as well as the first study of step-to-step fluctuations in these cells in any species. While natural movement is expected to produce variable neural responses, we wish to emphasize not the absolute magnitude of variability, but its rich statistical structure, which reveals several key insights. First, the variability expresses characteristic bias, amplitude, and phase motifs, which are consistent with the encoding of kinematic variables. Second, this variability is related to multiple movement parameters in a step-phase-dependent way.

Figure 15: Purkinje cell properties differ across cerebellar lobules V and VI. (A) Left: sagittal view of the cerebellum, highlighting lobules V (magenta) and VI (green). Right: percentage of cells in each lobule with more than one activity peak in the step cycle. 91% of lobule V Purkinje cells have multiple peaks in the step cycle, in comparison with only 55% in lobule VI. (B) Distribution of mean firing rates, step tuning (Kuiper's statistic), and the norms of the head posture coefficients  $\sqrt{\beta_{roll}^2 + \beta_{pitch}^2}$ , speed coefficients ( $|\beta_{speed}|$ ), acceleration coefficients ( $|\beta_{accel}|$ ), and EMG coefficients ( $|\beta_{EMG}|$ ), for Purkinje cells in lobules V and VI. Cells in lobule VI have higher firing rates, are more modulated by head posture, and are less modulated by acceleration than lobule V cells. (C) Joint distribution of firing rates, the norm of the acceleration coefficients, and the norm of the posture coefficients. These differences are consistent with a larger role for lobule V in limb control during locomotion, and for lobule VI in the control of the neck and head.

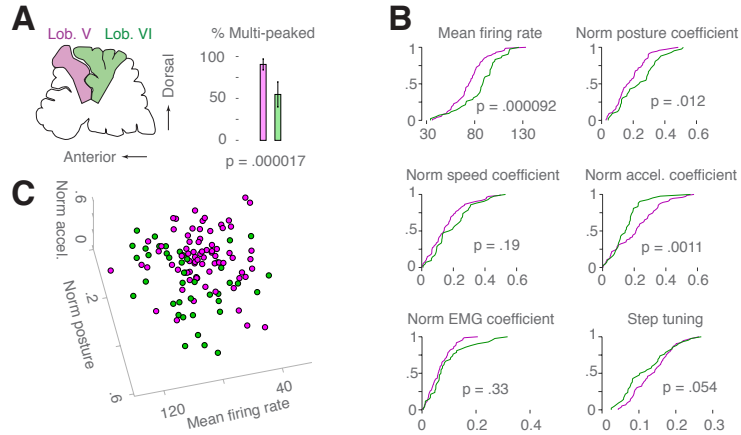
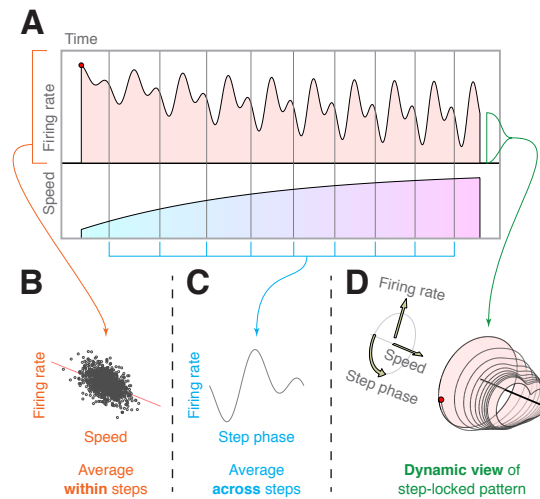


Figure 16: A dynamic view of neuronal activity during locomotion. **(A)** A schematic Purkinje cell with a step-locked pattern controlled by a single parameter, speed. Note the systematic transition in the firing rate curve as speed increases. **(B)** A view of the activity of the schematic neuron in **(A)** after averaging within steps. A relationship between speed and firing rate is apparent, but the dependence of activity on step phase within each cycle is obscured. **(C)** A view of the same neuron's activity after averaging across steps. While this view reveals the dependence of firing rate on step phase, it obscures step-to-step variability and its dependence on speed. **(D)** A dynamic view of the cell's step-locked firing pattern. Each step produces one full rotation around the speed axis, and as the animal's speed increases, the firing rate follows the trajectory from **(A)**, shown in gray. Under this view, the step-locked firing pattern is itself shaped by behavioral factors during locomotion, allowing flexible control of movement under dynamic conditions.



Third, an analysis of the phase-dependent regression curves reveals functional clusters of Purkinje cells: for instance, one group of cells is amplitude-modulated by speed, while another is phase-modulated by head roll. Fourth, the presence of step-to-step correlations for many pairs of cells, as well as correlations between behavior and spiking, suggests variability is not mainly due to intrinsic, single-neuron noise. Finally, there is a pronounced disassociation between patterns of variability driven by the parallel and climbing fiber systems, suggesting that they use qualitatively distinct coding schemes.

One limitation of our chronic, freely moving preparation is that it does not allow direct assessment of proprioceptive, vestibular, and somatosensory properties of neurons, which must be measured under much more controlled conditions (typically, head fixation and anesthesia). Furthermore, optical measurements of multi-joint kinematics are highly challenging in small animals freely navigating an environment. Thus, while we can establish a correspondence between neuronal activity and measured variables such as speed and head attitude, it is difficult to establish whether these are the primary variables encoded, or are simply correlated with other variables that drive the responses. However, in contrast with head fixed and treadmill-based designs, our approach allows a direct measurement of neuronal activity during the natural initiation, modulation, and termination of locomotion, and reveals much richer statistical structure in this activity than previously demonstrated.

Several factors could be responsible for the observed variability across steps. If Purkinje cells encoded kinematic variables such as joint angle, the neural variability might reflect variability in kinematics. For instance, at higher speeds of locomotion, joint angle excursions tend to be larger (Costa et al., 2010), and neural signals encoding angle should have larger amplitudes at higher speeds. Indeed, the strong amplitude modulation by speed observed for many cells (Figure 11C, D, E) is consistent with this hypothesis. Alternatively, the step-

to-step variability could reflect variation in external forces (Bernstein, 1967). In order to maintain a periodic movement trajectory, the nervous system must compute the difference between the desired periodic force profile and perturbations due to ground reaction forces, gravity, and other external sources. These external perturbations may be aperiodic and highly variable, and might consequently produce a neural difference signal that is much more variable than the movement itself. Our observation of step-locked firing profiles that varied considerably, even for consecutive steps (Figure 8B, 9), might result in part from the participation of Purkinje cells in this computation.

The behavior-dependent modification of the step-locked firing pattern likely enhances motor performance both directly, through feedforward routes to the spinal cord, and indirectly, by gating neocortical commands. The direct, feedforward pathways provide speed- and posture-dependent modification of motor parameters, such as the amplitude, duty cycle, and timing of muscle activity, while leaving the basic stepping rhythm intact. On the other hand, the indirect, gating pathway could coordinate cortically-initiated commands with locomotion, as when a walking animal needs to brake suddenly in response to a visual stimulus, correct a postural disturbance, or step over an obstacle. In order to execute these movements effectively, the descending control signals must meet two criteria. First, they must have an amplitude that scales with the animal's speed or posture across steps; for instance, at higher speeds, a larger braking signal is required to generate larger extensor forces and stop the animal. Second, they must be appropriately timed within the step cycle; a braking command that increases extensor activity during swing will likely cause the animal to stumble. These two criteria could be satisfied through a multiplicative interaction between a binary neocortical command and a cerebellar gating signal that depended on both step phase and speed. The resulting output would scale with the animal's speed, producing

larger braking forces when the animal moved faster. Crucially, it would also vary with step phase within each cycle, allowing braking to be initiated only during the correct part of the cycle. Thus, a cortical signal with a fixed amplitude initiated at an arbitrary speed and step phase would produce a descending control signal with the appropriate amplitude and timing.

Previous work in cats performing treadmill locomotion at two discrete speeds has demonstrated that step-averaged Purkinje cell firing rates tend to be higher at faster speeds (Armstrong and Edgley, 1988). Our results advance this work in four key respects. First, our use of continuous, natural variation in behavior over a wide range rather than at two discrete points allows us to precisely estimate the magnitude of behavioral effects on firing rate (Figure 11B). Second, our simultaneous measurement of several behavioral variables enables us to model the joint effects of these variables in the same cells (Figure 11C). Third, our estimation of phase-dependent regression curves demonstrates that behavioral variables do not merely produce changes in mean firing rate, but may also have effects that depend strongly on step phase (Figure 12A). Finally, our analysis of bias, amplitude, and phase scores for these regression curves reveals that the Purkinje cell population is not uniform, but highly heterogeneous, and exhibits functional clusters (Figure 12B). For instance, speed and pitch tend to influence either the bias or the amplitude of the firing rate curve, while acceleration and roll may modulate the phase. These results depend critically on our analysis of variability both across steps and within the step cycle, and would be obscured by averaging over either.

Our findings show that the parallel and climbing fiber systems convey different types of information to Purkinje cells during locomotion: simple spikes are modulated both within the step cycle (by step phase) and across steps (by speed and head posture), while complex

spikes show only moderate tuning within the step cycle, and no effect of behavioral variables across steps. In addition, the low Fano factors observed for complex spikes suggest that behavioral fluctuations during movement do not imply that neural responses will be variable throughout the motor system. These findings are consistent with the idea that the climbing fiber system conveys a sparse, impulse-like signal that shapes parallel fiber synaptic weights, but does not use an analog rate code for sensorimotor variables (Albus, 1971; Marr, 1969). However, because our experimental approach does not permit high-density sampling of complex spikes from Purkinje cells within the same microzone, our results do not rule out the possibility that locomotor parameters are encoded through complex spike synchrony, rather than rates. Indeed, recent calcium imaging studies have demonstrated that correlated complex spike activity increases significantly during locomotion relative to rest, particularly around movement onset (De Gruijl et al., 2014; Ozden et al., 2012), but that this increase does not occur in mice lacking connexin36, which is essential for gap junction coupling of olivary ensembles (De Gruijl et al., 2014). Furthermore, mice with P/Q-type calcium channel abnormalities exhibit a lack of microzonal complex spike synchrony and pronounced deficits in timing, accuracy, and interlimb coordination during stepping (Hoogland et al., 2015).

Although complex spikes were tuned to step phase for only a minority (12/65) of Purkinje cells, this result contrasts with previous work in the paravermis (Armstrong et al., 1988) and lateral vermis (Andersson and Armstrong, 1987) of awake, intact cats, which did not reveal statistically significant complex spike modulation during stepping. This discrepancy might be due to our analysis of a larger number of steps (mean of 1064 cycles, compared with approximately 100 cycles), or to our choice of statistical technique (a test based on the circular empirical distribution function, compared with a test based on histogram extrema).

The difference might also be due to the location of the recorded cells, which were more medial in our sample, or to our use of rats as experimental animals, instead of cats.

We observed large correlations between many pairs of simultaneously-recorded Purkinje cells, providing further evidence that step-to-step variability does not merely reflect intrinsic noise at the level of individual neurons, but is rather a result of coordinated inputs (Lee et al., 1998). These correlations are not simply due to similar tuning to speed, acceleration, and head posture, since they persist after removing the effects of these factors. Furthermore, the prevalence of both positive and negative partial correlations suggests that the coordination is not merely shared drive from the central pattern generator or from a single muscle or joint, but rather reflects cells' different weightings of a range of inputs. As previous studies in cerebral cortex have suggested (Averbeck and Lee, 2003; Lee et al., 1998; Maynard et al., 1999), the presence of correlations in ensemble activity might constrain the encoding of movement parameters.

Several overlapping pathways into lobules V and VI of the vermis are likely responsible for the influence of step phase, speed, acceleration, and head attitude on Purkinje cell activity. Proprioceptive and cutaneous information from the forelimbs and hindlimbs arrives through spinocerebellar and cuneocerebellar tracts (Adrian, 1943; Anderson, 1943; Matsushita and Hosoya, 1979; Snyder et al., 1978; Tolbert and Gutting, 1997), some of which also carry signals from the spinal rhythm generating network (Arshavsky et al., 1986). Information about head posture arrives through primary (Barmack et al., 1993) and secondary (Barmack et al., 1992; Kotchabhakdi and Walberg, 1978; Matsushita and Wang, 1987) vestibular projections and through the central cervical nucleus (Matsushita and Hosoya, 1979; Snyder et al., 1978), which receives both vestibular and neck proprioceptive signals (Popova et al., 1995; Thomson et al., 1996). The convergence of vestibular and propriocep-

tive pathways in the dorsal vermis is consistent with physiological studies (Jensen, 1985; Precht et al., 1977), which have identified individual Purkinje cells responsive to both neck and vestibular stimulation (Denoth et al., 1979; Manzoni et al., 1999). The modulation of Purkinje cell activity both within and across steps, then, likely reflects the integration of signals from diverse pathways and modalities.

Although Purkinje cells in both lobule V and lobule VI are modulated by step phase, speed, acceleration, and head posture, our data do provide evidence for functional differences between lobules. Cells in lobule V were more strongly influenced by acceleration and had multiple firing peaks in the step cycle, suggesting that they might control the activity of multiple joints, or of single joints undergoing multiple cycles of flexion and extension per step. Cells in lobule VI, on the other hand, were more strongly modulated by head posture than lobule V cells, suggesting that they help maintain the stability of the head during stepping.

Taken together, these results reveal several novel features of Purkinje cell activity during locomotion that would not have been apparent after averaging. The strategy of averaging within steps to obtain a scalar firing rate for each cycle (Figure 16B) has the advantage of revealing the relationship between behavioral variables and neuronal activity, but obscures the functionally critical (Arshavsky et al., 1986) and often complex dependence of activity on step phase. On the other hand, averaging across steps to obtain the phase-dependent firing rate (Figure 16C) obscures the extent and statistical structure of step-to-step variability, as well as step-to-step correlations between behavior and Purkinje cell activity, and between the firing rates of multiple neurons. Our findings suggest a dynamic view of neuronal activity during locomotion, in which a step-phase-dependent firing pattern is itself modulated by behavior during ongoing movement (Figure 16D).

### 3.5 Experimental Procedures

Three male Long-Evans rats were trained to walk for water reward on a 1.8m-long linear track. Three LEDs were fixed to the headstage, and animal position was monitored using an overhead camera with video acquisition timestamped on the same global clock as electrophysiological recordings. Head pitch and roll were estimated from data acquired with a headstage-mounted inertial measurement unit using a Kalman smoother. An EMG was acquired from the acromiotrapezius, as described in Chapter 2. Steps were identified by filtering the EMG with a 100-1000Hz finite impulse response filter, rectifying and smoothing the signals using a 100ms Gaussian kernel, then searching for sequences of peaks (local maxima) occurring during track traversal. Stepping sequences were required to include at least four peaks, with consecutive peaks separated by 220-450 ms. The step phase was obtained by linear interpolation, with the EMG peak defined as 0 for cells ipsilateral to the muscle and on the midline, and as  $\pi$  for contralateral cells. All animal procedures were in accordance with the National Institutes of Health (NIH) guidelines, and with the approval of the Caltech Institutional Animal Care and Use Committee. The animals were kept on a 12-hour light cycle, followed by 12 hours of darkness, and were run in two daily sessions: one approximately four hours into the light cycle, and one approximately four hours into the dark cycle.

Rats were chronically implanted with a 24-tetrode microdrive array, as described in Chapter 2. Spikes were clustered by fitting a mixture model in a 12-dimensional feature space (three waveform principal components per tetrode channel) (Calabrese and Paninski, 2011; Ecker et al., 2014; Tolias et al., 2007). For cells with large and stable complex spikes, an additional stage of processing was used to distinguish complex from simple spikes. The initial, fast segment of the complex spikes had the same amplitude ratios across tetrode

channels as the simple spikes for the same unit (de Solages et al., 2008), so that a single unit cluster for a Purkinje cell contained both simple and complex spikes. A matched filter for complex spikes was constructed by convolving a 25-30Hz finite impulse response filter with a decaying exponential function having a time constant of 5ms. This filter was applied to the raw, broadband data, and the peaks in the resulting signal were registered with the preceding spike from the corresponding unit cluster. The broadband waveforms were extracted within -2ms and 10ms of these putative complex spike events and sorted using principal component features. Thus, each spike in the unit cluster was identified as either simple or complex. For analyses that did not compare simple and complex spike activity, the cell’s spike train was taken to be the union of spikes of both types. At the end of each experiment, electrolytic lesions were applied at each recording site, and the tetrode locations were verified in Hoescht-stained tissue sections.

The state-dependent mean firing rates for locomotion, licking, and inactivity were defined as the total number of spikes occurring in the state divided by the total duration of the state throughout the dataset. For each Purkinje cell, a circular distribution was fit to the step phases sampled at the spike times. A second-order generalized von Mises distribution (Gatto and Jammalamadaka, 2007) was fit for cells with one or two peaks in the step cycle. For cells with three peaks, a kernel density estimator was used with a wrapped normal distribution of width  $(\frac{4}{3N})^{0.2}v$ , where  $v$  is the sample circular standard deviation (Mardia and Jupp, 2000). To determine whether spiking was locked to the step cycle, Kuiper’s test was used (Mardia and Jupp, 2000) for both simple and complex spikes. Lick modulation was determined using the same procedure, with the lick onset defined to be 0 degrees.

The step-to-step variability of spike counts was quantified using the variance-to-mean ratio, or Fano factor. For each neuron and window length  $\Delta t$ , the Fano factor was computed

as:

$$FF(\Delta t) = \frac{\text{var}(n(\Delta t))}{\text{mean}(n(\Delta t))}$$

where  $n(\Delta t)$  is the number of spikes lying within a window of length  $\Delta t$  ms following the EMG peak for each step.

The shape of the step-locked firing rate curves was investigated by smoothing the spike trains with a 25ms Gaussian kernel and extracting the curves for each step, with the time axis normalized so that each curve was parameterized by step phase  $\theta$ , rather than time. Principal component analysis was performed on the curves for each cell, and the effect of each component,  $w(\theta)$ , was visualized as a perturbation of the mean curve,  $f(\theta)$  (Ramsay and Silverman, 2005). The extent to which each component was an additive shift, a multiplicative scaling, or a phase shift was determined by computing bias, amplitude, and phase scores, respectively. A pure bias shift corresponds to a completely flat component, so the bias score was defined to be:

$$S_{bias} = |w(\theta) \bullet v(\theta)|$$

with  $v(\theta) = \frac{1}{\sqrt{n}}$ , where  $n = 50$  is the length of the curve. A pure shift in amplitude corresponds to a component with the same shape as the mean curve, but rescaled by a multiplicative constant. The amplitude score was defined using:

$$f^*(\theta) = \frac{f(\theta) - \mu_f}{\|f(\theta) - \mu_f\|}$$

$$S_{amp} = |w(\theta) \bullet f^*(\theta)|$$

where  $\mu_f$  is the mean of  $f(\theta)$ . A pure phase shift of  $\delta \neq 0$  would correspond to a transfor-

mation of  $f(\theta)$  to  $f(\theta + \delta)$ , so the phase score was defined using:

$$g_{\delta}(\theta) = \frac{f(\theta + \delta) - f(\theta)}{\|f(\theta + \delta) - f(\theta)\|}$$

$$S_{phase} = \max_{\delta \in (-\Delta, \Delta) \setminus \{0\}} |w(\theta) \bullet g_{\delta}(\theta)|$$

where  $\Delta = 22^{\circ}$ . The range of possible offsets was limited to  $2\Delta$  in order to regularize the phase score estimation.

The influence of behavioral variables on Purkinje cell activity across steps was first determined by averaging speed, forward acceleration,  $\sin(\text{roll})$ , and  $\sin(\text{pitch})$ , and EMG amplitude within each step cycle. Larger values of pitch reflect upward movement of the head (dorsiflexion). Positive values of roll correspond to rightward rotations of the head for cells on the right side, and to leftward rotation for cells on the left side and midline. To study the variation in curve shape with behavior, slicing intervals for behavioral values were determined using an equal-count algorithm with twelve (Figure 11D) or six (Figure 11E) intervals and 50% overlap (Cleveland, 1993). Step-locked firing rates were then averaged within each interval.

In order to quantify the influence of behavior on spiking, we defined the firing rate on each step to be the number of spikes occurring during that step divided by the step duration. We converted the firing rate and the behavioral variables to z-scores, and estimated a multiple regression model for each cell:

$$Z_{rate} = \beta_{speed}Z_{speed} + \beta_{acc}Z_{acc} + \beta_{roll}Z_{roll} + \beta_{pitch}Z_{pitch} + \beta_{EMG}Z_{EMG} + \epsilon$$

where  $Z_{rate}$  is the z-score of the step-locked firing rates,  $Z_{roll}$  is the z-score of  $\sin(\text{roll})$ ,  $Z_{pitch}$

is the  $z$ -score of  $\sin(\text{pitch})$ ,  $Z_{EMG}$  is the  $z$ -score of the EMG amplitude, and  $\epsilon$  is a normally-distributed error term. The normality of the residuals was checked using quantile-quantile plots. Performing the same analysis using rank-transformed data, substituting the  $z$ -scored ranks of the independent and dependent variables for the original linear data, produced nearly identical parameter estimates.

In order to study how the relationship between neural activity and behavior varies throughout the step cycle, we next estimated step-phase-dependent regression curves (Figure 12A). For each step phase  $\theta$ , we estimated the following model:

$$Z_{rate}(\theta) = \beta_{speed}(\theta)Z_{speed}(\theta) + \beta_{acc}(\theta)Z_{acc}(\theta) + \beta_{roll}(\theta)Z_{roll}(\theta) + \beta_{pitch}(\theta)Z_{pitch}(\theta) + \beta_{EMG}(\theta)Z_{EMG}(\theta) + \epsilon$$

where  $Z_{rate}(\theta)$  is firing rate at phase  $\theta$ ,  $z$ -scored with respect to the distribution of firing rates at  $\theta$ , and  $Z_{speed}(\theta)$  is the  $z$ -scored speed at  $\theta$ .

We characterized the shape of these regression curves by computing scores for bias ( $S_{bias}$ ), amplitude ( $S_{amp}$ ), and phase ( $S_{phase}$ ), by substituting  $\frac{\beta_{var}(\theta)}{\|\beta_{var}(\theta)\|}$  for  $w(\theta)$  for each behavioral variable. This produced an ordered triplet ( $S_{bias}, S_{amp}, S_{phase}$ ) for each significantly tuned cell ( $\beta_{var} \neq 0$  at  $q = .05$ ). For each behavioral variable, we performed an agglomerative hierarchical clustering analysis of these triplets using a Ward linkage function and a gap criterion for determining the number of clusters (Everitt, 2011).

Coordinated activity between pairs of cells was assessed using the partial rank correlations in the firing rates: the effects of the behavioral variables were first removed using the multiple regression model, and Spearman's  $\rho$  was computed between the residuals. Partial rank correlations computed using the residuals from the rank-transformed regression model produced nearly identical correlations.

The low rate of complex spikes did not permit the analysis of step-locked firing rates; instead, we studied the effects of behavioral variables on the number of complex spikes,  $C$ , within a 350ms window starting at the onset of each step cycle. For each Purkinje cell with stable complex spikes, we estimated a Poisson regression model:

$$\log(E(C|Z_{speed}, Z_{roll}, Z_{pitch})) = \mu_C + \beta_{speed}Z_{speed} + \beta_{acc}Z_{acc} + \beta_{roll}Z_{roll} + \beta_{pitch}Z_{pitch} + \beta_{EMG}Z_{EMG} + \epsilon$$

where  $\mu_C$  is the mean number of spikes, and  $Z_{speed}$ ,  $Z_{acc}$ ,  $Z_{roll}$ ,  $Z_{pitch}$ ,  $Z_{EMG}$ , and  $\epsilon$  are defined as in the previous equation.

For the analysis of step phase and lick modulation, the linear models, and the pairwise correlations, corrections for multiple comparisons were made by setting the false discovery rate to  $q = .05$  (Benjamini and Hochberg, 1995). Data from all animals, Purkinje cells, and steps were included in the analysis. For parametric tests, the assumption of normality was checked using normal quantile-quantile plots.

## 4 State-Dependent Firing Patterns in Cerebellar Purkinje Cells during Sleep

*He had ideas of decency which went back to the novels of Dickens,  
but he had wicked REMs ...  
- Saul Bellow, Ravelstein*

### 4.1 Summary

Purkinje cells constitute the sole output of the cerebellar cortex, but little is known about how their firing patterns evolve over natural sleep. Here, we obtain recordings from Purkinje cells in unrestrained adult rats during sleep, along with electromyograms and local field potentials in the cerebellar cortex, neocortex, and hippocampus. We find that the rates of simple spikes, which are driven by the mossy-parallel fiber system, and complex spikes, driven by the climbing fiber system, are attenuated during sleep. Although firing rates during slow wave sleep (SWS) and rapid eye movement sleep (REM) are similar, simple spike activity is highly regular in SWS, while REM is characterized by phasic increases and pauses in simple spiking. This phasic activity in REM is associated with pontine waves, which propagate into the cerebellar cortex and modulate both simple and complex spiking. Such a temporal coincidence between simple and complex spikes is known to drive synaptic plasticity at parallel fiber synapses; consequently, pontocerebellar waves may provide a mechanism for tuning synaptic weights in the cerebellum during active sleep.

### 4.2 Introduction

The cerebellar cortex is a major supraspinal center involved in motor control and learning, and two main pathways provide excitation to its principal neurons, the Purkinje cells (Eccles et al., 1967). The first pathway originates in cerebellar granule cells, which integrate mossy

fiber signals from the brainstem and spinal cord, converge onto Purkinje cells through the parallel fibers, and regulate the rate of simple spikes. The second pathway originates in the inferior olivary nuclei, which send climbing fibers to the cerebellar cortex and regulate complex spiking. The climbing fiber system is critical for regulating heterosynaptic plasticity at parallel fiber synapses: simultaneous activation of the parallel and climbing fibers induces long-term depression, while the unpaired activation of parallel fibers tends to result in potentiation (Ito, 2001).

While the firing properties of Purkinje cells have been studied using a wide range of motor tasks and animal models, little is known about activity patterns during natural sleep. In mammals, sleep consists of two principal stages: slow wave sleep (SWS), and active, or rapid eye movement sleep (REM). During SWS, blood pressure and heart rate are depressed, skeletal muscle tone is maintained, neocortical slow oscillations (1-4Hz) are apparent in the local field potential (LFP), and sharp wave ripples occur in the hippocampus. In REM, by contrast, muscle tone is suppressed, metabolic rates increase, phasic twitches and rapid eye movements occur, and the hippocampal LFP is dominated by theta oscillations (4-10Hz). Another prominent characteristic of REM is the occurrence of pontine waves, which were first described in cats as ponto-geniculo-occipital (PGO) waves, due to their propagation into visual cortex via the thalamus (Bizzi and Brooks, 1963; Jeannerod et al., 1965). Subsequent studies revealed that these waves occur in other species, including rats (Kaufman and Morrison, 1981; Marks et al., 1980a), are generated by high-frequency bursts in pontine neurons (McCarley et al., 1978), and spread into a wide range of brain areas, including the cerebellum (Marks et al., 1980b; Pellet and Harlay, 1977; Pellet et al., 1974). Furthermore, they coincide with an increase in the frequency of hippocampal theta oscillations (Karashima et al., 2002; Karashima et al., 2005), are associated with muscle

twitches and rapid eye movements, and can be evoked by acoustic stimuli during quiet wakefulness and SWS (Kaufman and Morrison, 1981).

Single-unit recordings from Purkinje cells during sleep have been obtained in cats and monkeys, and several studies have reported differences in simple and complex spike rates between SWS and REM; increases in the rate of simple and complex spikes have been documented during REM in cats (Hobson and McCarley, 1972; Marchesi and Strata, 1970), though a suppression of complex spikes during REM has been reported in monkeys (Mano, 1970). Furthermore, studies in developing rats have shown that myoclonic twitch is associated with increases in both simple and complex spiking (Sokoloff et al., 2015a; Sokoloff et al., 2015b); remarkably, this modulation is present as early as P4, when the parallel fiber system is undeveloped and mossy fibers make transient, functional connections directly onto Purkinje cells. It is unclear from previous work, however, how the activity of Purkinje cells depends on sleep state in adult rodents, and we address two open questions in the present study. First, how do simple and complex spike firing patterns evolve across sleep in adult rats, and are differences between SWS and REM restricted to changes in mean firing rate, or do higher-order changes in spike train statistics occur? Second, how do pontocerebellar waves influence the parallel and climbing fiber systems during REM sleep? This question is central to the problem of cerebellar plasticity during sleep, as the synchronous activation of these two pathways is known to induce changes in the strength of parallel fiber synapses.

### 4.3 Results

We performed simultaneous recordings of hippocampal, neocortical, and cerebellar local field potentials (LFP) in conjunction with electromyography (EMG) and recordings from cerebellar Purkinje cells ( $n = 39$ ) in chronically implanted, naturally sleeping adult rats ( $n$

= 3). Using hippocampal and cortical LFPs and EMG, we segmented the datasets into episodes of waking (WK), slow wave sleep (SWS), and rapid eye movement sleep (REM; Figure 17C, left panel and below). During SWS, the hippocampal LFP exhibited large irregular activity and sharp wave ripples, slow waves were visible on the cortical LFP, and a moderate level of tonic EMG was apparent (Figure 17A). By contrast, REM was characterized by prominent hippocampal theta oscillations, an attenuation of cortical slow waves, and a suppression of muscle tone below the SWS baseline (Figure 17B). Throughout these extended sleep sessions, it was possible to maintain stable recordings of simple and complex spikes from Purkinje cells in the cerebellar vermis, and spike amplitudes (Figure 17D, above) and waveforms (Figure 17D, below) were steady for the duration of the sessions.

In order to characterize the dependence of Purkinje cell activity on global changes in brain state, we first compared the mean firing rates for each cell during WK, SWS, and REM (Figure 18A). The rates of both simple (Figure 18A, above) and complex spikes (Figure 18A, below) were attenuated during SWS and REM, relative to WK (paired t-tests,  $p < .05$ ; simple spike means for WK, SWS, and REM: 57.7, 54.1, 54.5; complex spike means: 1.34, 1.17, 1.23). However, while a few cells had much higher firing rates during REM than SWS, we detected no difference in the mean rates for the two sleep states across the sample of cells.

Although the mean firing rates during SWS and REM were similar, we observed more subtle differences in spike train structure between the states: simple spiking tended to be highly regular during SWS (Figure 17A), but exhibited prominent pauses and phasic increases during REM (Figure 17B). We quantified this difference by estimating J-functions for the state-dependent simple spike trains (see Experimental Procedures). The J-function describes the degree of regularity or clustering in a point pattern as a function of the

Figure 17: State detection and single-unit Purkinje cell recording during extended sleep sessions. (Continued on the following page.)

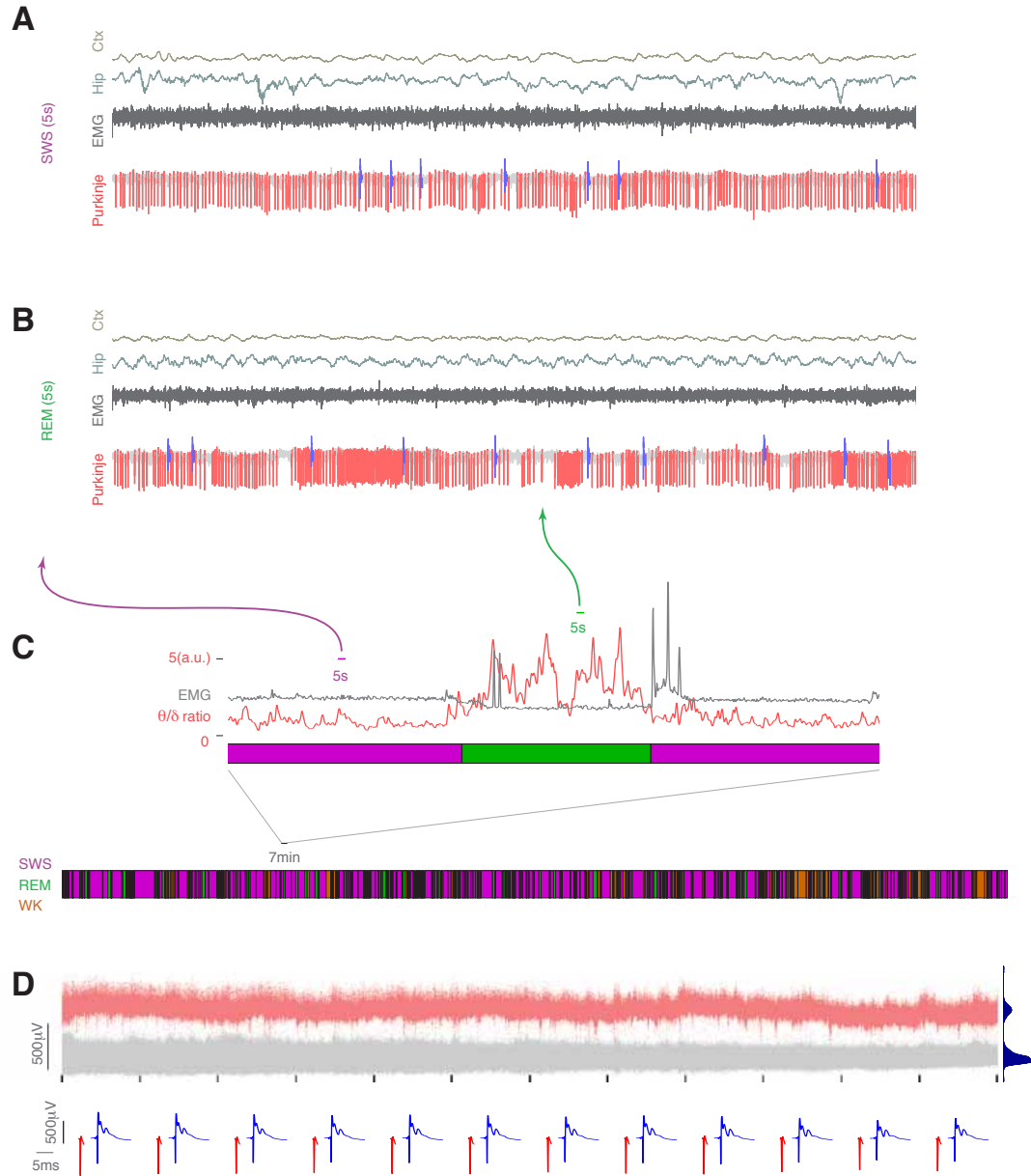
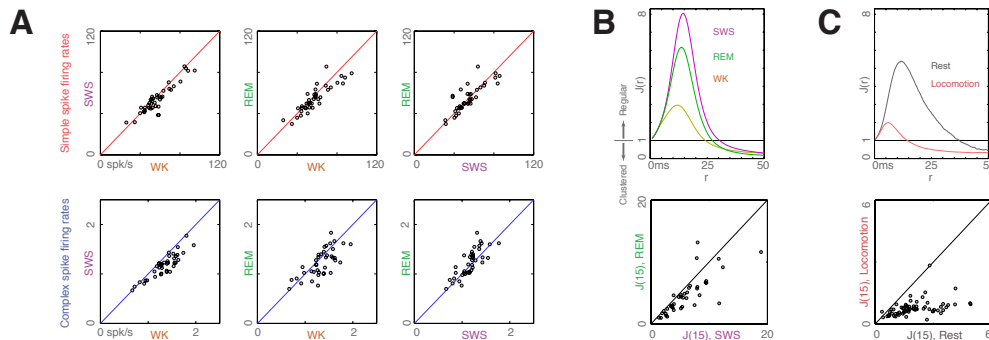


Figure 17: **(A)** Hippocampal LFP, neocortical LFP, acromiotrapezius EMG, and raw Purkinje cell data during five seconds of SWS. Note the cortical slow oscillations, hippocampal sharp waves, muscle tone, and homogeneous, regular simple spiking. **(B)** Raw data for five seconds of REM. In contrast with SWS, cortical slow waves are absent, the hippocampal LFP is dominated by theta oscillations, muscle tone is suppressed, and Purkinje cell spiking is irregular and phasic. **(C)** Above: changes in the ratio of hippocampal theta amplitude to neocortical slow wave amplitude (red) along with EMG power (gray) around an episode of REM sleep. Below: segmentation of the full 16-hour dataset into episodes of slow wave sleep (magenta), rapid eye movement sleep (green), and waking (orange). **(D)** Above: stability of Purkinje cell spike amplitudes throughout the 16-hour session in **(C)**. Spike amplitudes for the Purkinje cell on a single tetrode channel are red, amplitudes for the multi-unit cluster are gray, and the blue histogram shows the full amplitude distribution. Below: simple (red) and complex spike (blue) waveforms for twelve equally-spaced segments of the dataset are stable throughout.

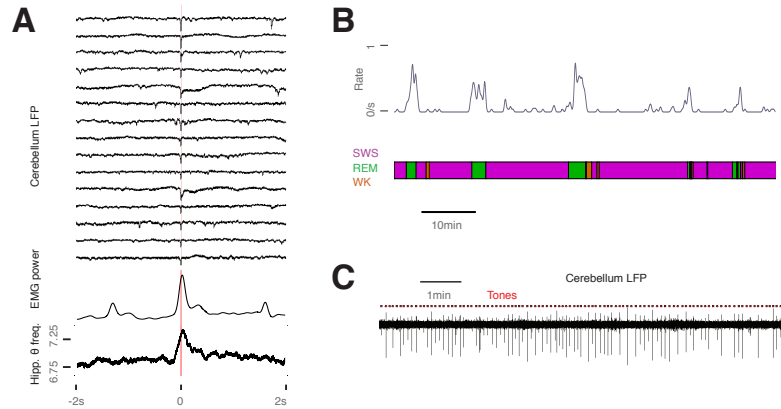
Figure 18: State-dependent simple and complex spike rates. **(A)**: Average firing rates for pairs of states. Top row: simple spikes. Bottom row: complex spikes. **(B)**: Simple spike activity is more regular in SWS than REM. Above: state-dependent J-functions for an example cell. These functions indicate the degree of regularity or clustering at a given interaction distance. Larger values suggest greater regularity in spike trains, while smaller values suggest clustering. Below: J-function values, evaluated at a 15ms interaction distance, for REM vs SWS. **(C)**: State-dependent J-functions for an example cell (above) and J-function values at 15ms (below) during locomotion and inactivity for a separate sample of Purkinje cells ( $n = 65$ ).



interaction distance,  $r$ . Values of  $J(r)$  larger than one indicate that the pattern is regular (periodic or lattice-like), while smaller values suggest clustering (e.g. phasic bursts). An examination of the  $J$ -functions for simple spikes during SWS and REM revealed two key features (Figure 18B, above). First, the spike trains during both states were typically regular at short interaction distances (0ms to approximately 25ms), but clustered at longer distances (greater than 25ms). Second, spike trains were significantly more regular during SWS than during REM (Figure 18B, below;  $p = .0002$ , paired t-test), consistent with the observation of more phasic activity in REM (compare with fig. 1A, center and right). This difference between SWS and REM was paralleled during awake behavior: using a separate dataset obtained from Purkinje cells during locomotion on a linear track (Sauerbrei et al., 2015), we estimated the  $J$ -functions for simple spike trains during walking and awake inactivity, and observed a higher degree of regularity during rest than locomotion (Figure 18C;  $p < 10^{-20}$ , paired t-test). The higher spiking regularity during resting than locomotion and during SWS than REM is consistent with the active, phasic nature of both motor behavior and REM.

Phasic modulation of simple spikes during REM occurs in the absence of voluntary movement; what internal events drive this phasic activity? An examination of the cerebellar LFP revealed sporadic, monophasic waves, which occurred intermittently during REM (Figure 19A, above). Four criteria established that these events corresponded to pontine waves propagating into the cerebellar cortex. First, the waves were concentrated around REM epochs (Figure 19B) and the transitions between SWS and REM, but were rarely detected during waking or early in SWS (Figure 19B). Second, they coincided with an increase in muscle activity (Figure 19A, middle), which was driven by occasional wave-locked twitches. Third, they were associated with a speedup of the hippocampal theta rhythm

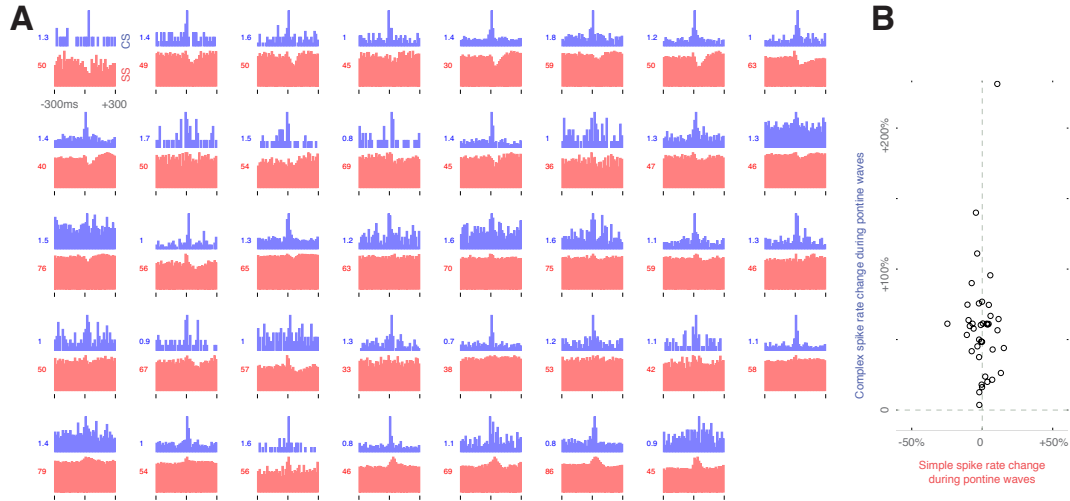
Figure 19: Detection of pontocerebellar waves. **(A)**: Raw cerebellar LFPs centered on spontaneous waves detected during REM sleep (above, sorted by amplitude), along with EMG power (middle) and hippocampal theta frequency (below). Notice that hippocampal theta frequency increases around pontocerebellar waves. **(B)**: Pontocerebellar wave rates (above) across sleep states (below). The waves are concentrated around REM epochs. **(C)**: Evoked pontocerebellar waves during auditory stimulation in SWS. Tones consistently evoke pontocerebellar waves with variable amplitudes.



during REM sleep (Figure 19A, below). Finally, similar waves could be evoked by acoustic stimuli during quiet wakefulness and SWS; these waves occurred on most stimulation trials, but varied in amplitude (Figure 19C).

Because the pontocerebellar waves detected in the LFP are driven by afferent mossy fiber activity, they might be expected to drive changes in simple spike rates, which are regulated by the mossy-parallel fiber pathway onto Purkinje cells and by feedforward inhibition through molecular layer interneurons. Indeed, many Purkinje cells exhibited increases ( $n = 9$ ) or decreases ( $n = 11$ ) in simple spike rates in a window of  $\pm 100$ ms (Figure 20A;  $p < .05$ , paired t-test). Furthermore, complex spike rates were modulated for most neurons ( $n = 28$ , Figure 20A), suggesting that pontocerebellar waves propagate into cerebellar cortex not only through mossy fibers, but also through the climbing fibers, via the inferior olive. In contrast with simple spikes, which were enhanced during pontocerebellar waves for some cells but suppressed for others, complex spikes exhibited only rate increases (Figure

Figure 20: Modulation of simple and complex spike firing during pontocerebellar waves. **(A)**: peri-wave event histograms for simple (red) and complex spikes (blue). Mean simple and complex spike rates during REM are indicated for each cell. **(B)**: Changes in complex versus simple spike firing rates in a window of -100ms to +100ms centered on pontocerebellar waves, with respect to a preceding window of -300ms to -100ms.



20B).

#### 4.4 Discussion

The present study uses chronically implanted multi-electrode arrays in the cerebellum, hippocampus, and neocortex in conjunction with electromyography to study patterns of Purkinje cell activity in sleeping rats. We find that simple and complex spike activity are both attenuated during sleep relative to waking, though the differences in firing rates between SWS and REM are typically small. The temporal structure of simple spiking differs markedly between the two states of sleep, however, with greater regularity in SWS and more phasic activity in REM. This phasic activity is associated with pontocerebellar waves, which concurrently modulate both simple and complex spikes in a temporal window of approximately  $\pm 100$ ms.

The observation of pontocerebellar waves in cerebellar cortex is consistent with a large

number of anatomical studies, which have documented the presence of mossy fiber projections from the pontine nuclei into the vermis in a range of species, including cats and rodents. Although pontocerebellar projections are denser in more lateral regions of cerebellar cortex, they are distributed across large areas of the vermis, including the anterior lobe and lobule VI. Pontine waves may also provide neuromodulatory input to the cerebellar cortex during REM: the locus coeruleus, which sends noradrenergic fibers into the cerebellum, is known to exhibit robust pontine waves in active sleep (Marks et al., 1980b).

Why did some Purkinje cells in our sample increase their simple spike rates around pontocerebellar waves, while others showed a decrease? One possible explanation is that granule cells activated during the events engage Purkinje cells not only through monosynaptic excitation from parallel fibers synapses, but also disynaptic, feedforward inhibition through molecular layer interneurons. Whether a given Purkinje cell has a net increase or decrease in firing, then, should depend on the relative weighting of interneuronal inhibition and parallel fiber excitation from granule cells; because this balance of excitation and inhibition likely varies across Purkinje cells, the sign and magnitude of the simple spike response might be expected to vary, as well.

The Marr-Albus-Ito theory posits that the central function of the climbing fiber system is to tune parallel fiber synaptic weights (Albus, 1971; Marr, 1969); this occurs largely through long-term depression at parallel fiber synapses that are co-activated along with the cell's climbing fiber input, though other types of plasticity have been reported, as well (Hansel et al., 2001; Ito, 2001). This theory, however, has been applied primarily in the domain of motor control in awake, behaving animals. Our observation that pontocerebellar waves concurrently engage both the parallel and climbing fiber systems within the window of plasticity suggests that a similar tuning of synaptic weights may occur during active sleep.

Indeed, it has been suggested that one role of REM is to adjust the strength of synapses in the neocortex (Crick and Mitchison, 1983), and the joint control of parallel and climbing fibers by pontine ensembles may serve a similar function in cerebellar circuits.

## 4.5 Experimental Procedures

Three adult male Long-Evans rats were chronically implanted with multi-tetrode microdrive arrays and electromyographic (EMG) electrodes, as described in Chapter 2 and Chapter 3.5. We recorded from 39 Purkinje cells during sleep, all of which had stable simple and complex spikes throughout the session; units with low-amplitude or unstable waveforms were not included in the analysis. For the comparison of spike patterns during locomotion and awake inactivity, we analyzed an additional dataset of 65 cells recorded as the animals walked for liquid reward on a linear track (Chapter 3).

Datasets were segmented into episodes of waking, slow wave sleep (SWS), and rapid eye movement sleep (REM) using the amplitude of the theta-band hippocampal LFP (4-10Hz passband), the ratio of the amplitudes of the theta to the delta-band cortical LFP (0-4Hz), and the EMG amplitude (100-1000Hz), as described previously (Wierzynski et al., 2009). Pontocerebellar waves were detected by filtering the cerebellar local field potential (13-85Hz) and detecting threshold-exceeding peaks separated by at least 200ms. Differences in mean firing rates across the sample of Purkinje cells were detected using paired t-tests for each pair of states. In order to characterize the structure of simple spike activity, we estimated J-functions for the spike trains in each behavioral state (Van Lieshout and Baddeley, 1996). At a given interaction distance  $r$ , the J-function is defined to be

$$J(r) = \frac{(1 - G(r))}{(1 - F(r))}$$

where  $G(r)$  is the probability that the nearest neighbor of a spike is closer than  $r$ , and  $F(r)$  is the fraction of the dataset occupied by the union of intervals of width  $2r$  centered at the spike times.  $J(r)$  is identically one for a homogeneous Poisson process. The value  $J(r)$  indicates the degree of regularity in the spike train at the interaction distance of  $r$ : larger values correspond to more regular (i.e., periodic or lattice-like) patterns, while values less than unity indicate clustering. Boundary effects were corrected by stitching together spike trains in consecutive episodes of a given type. Spike modulation around pontocerebellar waves was assessed using a paired t-test on the spike counts between  $-100$  and  $+100$ ms, compared with the counts between  $-300$  and  $-100$ ms. The magnitude of this modulation was defined to be the mean difference in spike counts in the two windows, divided by the product of the mean firing rate for the cell and the window duration of  $200$ ms.

## References

- Adrian, E. (1943). Afferent Areas in the Cerebellum Connected with the Limbs. *Brain* 66, 289-315.
- Albus, J. (1971). A theory of cerebellar function. *Mathematical Biosciences* 10, 25-61.
- Alisky, J.M., and Tolbert, D.L. (1997). Quantitative analysis of converging spinal and cuneate mossy fibre afferent projections to the rat cerebellar anterior lobe. *Neuroscience* 80, 373-388.
- Anderson, R.F. (1943). Cerebellar Distribution of the Dorsal and Ventral Spino-Cerebellar Tracts in the White Rat. *The Journal of Comparative Neurology* 79, 415-423.
- Andersson, G., and Armstrong, D.M. (1987). Complex spikes in Purkinje cells in the lateral vermis (b zone) of the cat cerebellum during locomotion. *The Journal of Physiology*, 107-134.
- Apps, R., and Hawkes, R. (2009). Cerebellar cortical organization: a one-map hypothesis. *Nature Reviews Neuroscience* 10, 670-681.
- Armstrong, D.M. (1988). The supraspinal control of mammalian locomotion. *The Journal of Physiology* 405, 1-37.
- Armstrong, D.M., and Edgley, S.A. (1984). Discharges of Purkinje cells in the paravermal part of the cerebellar anterior lobe during locomotion. *The Journal of Physiology*, 403-424.
- Armstrong, D.M., and Edgley, S.A. (1988). Discharges of interpositus and Purkinje cells of the cat cerebellum during locomotion under different conditions. *The Journal of Physiology* 400, 425-445.
- Armstrong, D.M., Edgley, S.A., and Lidiérth, M. (1988). Complex spikes in Purkinje cells of the paravermal part of the anterior lobe of the cat cerebellum during locomotion. *The Journal of Physiology*, 405-414.
- Arshavsky, Y.I., Gelfand, I.M., and Orlovsky, G.N. (1986). *Cerebellum and rhythmical movements* (Berlin; New York: Springer-Verlag).
- Arshavsky, Y.I., Orlovsky, G.N., and Popova, L.B. (1984). Activity of cerebellar Purkinje cells during fictitious scratch reflex in the cat. *Brain research* 290, 33-41.
- Averbeck, B.B., Latham, P.E., and Pouget, A. (2006). Neural correlations, population coding and computation. *Nature Reviews Neuroscience* 7, 358-366.

- Averbeck, B.B., and Lee, D. (2003). Neural noise and movement-related codes in the macaque supplementary motor area. *The Journal of Neuroscience* 23, 7630-7641.
- Barbour, B. (1993). Synaptic currents evoked in Purkinje cells by stimulating individual granule cells. *Neuron* 11, 759-769.
- Barmack, N.H., Baughman, R.W., Eckenstein, F.P., and Shojaku, H. (1992). Secondary vestibular cholinergic projection to the cerebellum of rabbit and rat as revealed by choline acetyltransferase immunohistochemistry, retrograde and orthograde tracers. *The Journal of Comparative Neurology* 317, 250-270.
- Barmack, N.H., Baughman, R.W., Errico, P., and Shojaku, H. (1993). Vestibular primary afferent projection to the cerebellum of the rabbit. *The Journal of Comparative Neurology* 327, 521-534.
- Barmack, N.H., and Yakhmitsa, V. (2003). Cerebellar climbing fibers modulate simple spikes in Purkinje cells. *The Journal of Neuroscience* 23, 7904-7916.
- Benjamini, Y., and Hochberg, Y. (1995). Controlling the False Discovery Rate - a Practical and Powerful Approach to Multiple Testing. *Journal of The Royal Statistical Society Series B* 57, 289-300.
- Berke, J.D., Okatan, M., Skurski, J., and Eichenbaum, H.B. (2004). Oscillatory entrainment of striatal neurons in freely moving rats. *Neuron* 43, 883-896.
- Bernstein, N.A. (1967). *The co-ordination and regulation of movements*, 1st English edition (Oxford; New York: Pergamon Press).
- Bizzi, E., and Brooks, D.C. (1963). Functional Connections between Pontine Reticular Formation and Lateral Geniculate Nucleus during Deep Sleep. *Archives Italiennes de Biologie* 101, 666-680.
- Bosco, G., and Poppele, R.E. (2001). Proprioception from a spinocerebellar perspective. *Physiological Reviews* 81, 539-568.
- Brochu, G., Maler, L., and Hawkes, R. (1990). Zebrin II: a polypeptide antigen expressed selectively by Purkinje cells reveals compartments in rat and fish cerebellum. *The Journal of Comparative Neurology* 291, 538-552.
- Calabrese, A., and Paninski, L. (2011). Kalman filter mixture model for spike sorting of non-stationary data. *Journal of Neuroscience Methods* 196, 159-169.
- Cao, Y., Maran, S.K., Dhamala, M., Jaeger, D., and Heck, D.H. (2012). Behavior-related pauses in simple-spike activity of mouse Purkinje cells are linked to spike rate modulation.

The Journal of Neuroscience 32, 8678-8685.

Chaisanguanthum, K.S., Shen, H.H., and Sabes, P.N. (2014). Motor variability arises from a slow random walk in neural state. *The Journal of Neuroscience* 34, 12071-12080.

Chambers, W.W., and Sprague, J.M. (1955). Functional localization in the cerebellum. I. Organization in longitudinal cortico-nuclear zones and their contribution to the control of posture, both extrapyramidal and pyramidal. *The Journal of Comparative Neurology* 103, 105-129.

Churchland, M.M., Yu, B.M., Cunningham, J.P., Sugrue, L.P., Cohen, M.R., Corrado, G.S., Newsome, W.T., Clark, A.M., Hosseini, P., Scott, B.B., et al. (2010). Stimulus onset quenches neural variability: a widespread cortical phenomenon. *Nature Neuroscience* 13, 369-378.

Churchland, M.M., Yu, B.M., Ryu, S.I., Santhanam, G., and Shenoy, K.V. (2006). Neural variability in premotor cortex provides a signature of motor preparation. *The Journal of Neuroscience* 26, 3697-3712.

Cleveland, W.S. (1993). *Visualizing data* (Murray Hill, N.J.: AT&T Bell Laboratories).

Costa, L.M., Pereira, J.E., Filipe, V.M., Couto, P.A., Magalhaes, L.G., Bulas-Cruz, J., Mauricio, A.C., Geuna, S., and Varejao, A.S. (2010). The effect of gait speed on three-dimensional analysis of hindlimb kinematics during treadmill locomotion in rats. *Reviews in the Neurosciences* 21, 487-497.

Crepel, F., and Jaillard, D. (1991). Pairing of pre- and postsynaptic activities in cerebellar Purkinje cells induces long-term changes in synaptic efficacy in vitro. *The Journal of Physiology* 432, 123-141.

Crick, F., and Mitchison, G. (1983). The function of dream sleep. *Nature* 304, 111-114.

Davie, J.T., Clark, B.a., and Husser, M. (2008). The origin of the complex spike in cerebellar Purkinje cells. *The Journal of Neuroscience* 28, 7599-7609.

De Gruijl, J.R., Hoogland, T.M., and De Zeeuw, C.I. (2014). Behavioral correlates of complex spike synchrony in cerebellar microzones. *The Journal of Neuroscience* 34, 8937-8947.

de Solages, C., Szapiro, G., Brunel, N., Hakim, V., Isope, P., Buisseret, P., Rousseau, C., Barbour, B., and Lna, C. (2008). High-frequency organization and synchrony of activity in the purkinje cell layer of the cerebellum. *Neuron* 58, 775-788.

Denoth, F., Magherini, P.C., Pompeiano, O., and Stanojevic, M. (1979). Responses of Purkinje cells of the cerebellar vermis to neck and macular vestibular inputs. *Pflugers*

Archiv 381, 87-98.

Dow, R.S., and Moruzzi, G. (1958). *The physiology and pathology of the cerebellum* (Minneapolis: University of Minnesota Press).

Eccles, J.C., Ito, M., and Szentgothai, J.N. (1967). *The cerebellum as a neuronal machine* (Berlin, New York: Springer-Verlag).

Eccles, J.C., Llinas, R., and Sasaki, K. (1966). The excitatory synaptic action of climbing fibers on the Purkinje cells of the cerebellum. *The Journal of Physiology* 182, 268-296.

Eccles, J.C., Oscarsson, O., and Willis, W.D. (1961). Synaptic Action of Group I and II Afferent Fibres of Muscle Spindles on the Cells of the Dorsal Spinocerebellar Tract. *The Journal of Physiology*, 517-543.

Ecker, A.S., Berens, P., Cotton, R.J., Subramaniyan, M., Denfield, G.H., Cadwell, C.R., Smirnakis, S.M., Bethge, M., and Tolias, A.S. (2014). State Dependence of Noise Correlations in Macaque Primary Visual Cortex. *Neuron* 82, 235-248.

Edgley, S.A., and Lidieth, M. (1987). The discharges of cerebellar Golgi cells during locomotion in the cat. *The Journal of Physiology* 392, 315-332.

Edgley, S.A., and Lidieth, M. (1988). Step-Related Discharges of Purkinje-Cells in the Paravermal Cortex of the Cerebellar Anterior Lobe in the Cat. *The Journal of Physiology* 401, 399-415.

English, A.W. (1978). An electromyographic analysis of forelimb muscles during overground stepping in the cat. *The Journal of Experimental Biology* 76, 105-122.

Everitt, B. (2011). *Cluster analysis*, 5th edn (Chichester, West Sussex, U.K.: Wiley).

Fedirchuk, B., Stecina, K., Kristensen, K.K., Zhang, M., Meehan, C.F., Bennett, D.J., and Hultborn, H. (2013). Rhythmic activity of feline dorsal and ventral spinocerebellar tract neurons during fictive motor actions. *The Journal of Neurophysiology* 109, 375-388.

Flusberg, B.A., Nimmerjahn, A., Cocker, E.D., Mukamel, E.A., Barretto, R.P., Ko, T.H., Burns, L.D., Jung, J.C., and Schnitzer, M.J. (2008). High-speed, miniaturized fluorescence microscopy in freely moving mice. *Nature Methods* 5, 935-938.

Fujita, H., Aoki, H., Ajioka, I., Yamazaki, M., Abe, M., Oh-Nishi, A., Sakimura, K., and Sugihara, I. (2014). Detailed expression pattern of aldolase C (Aldoc) in the cerebellum, retina and other areas of the CNS studied in Aldoc-Venus knock-in mice. *PLoS One* 9, e86679.

- Gao, H., Solages, C.D., and Lena, C. (2012). Tetrode recordings in the cerebellar cortex. *The Journal of Physiology (Paris)* 106, 128-136.
- Gatto, R., and Jammalamadaka, S.R. (2007). The generalized von Mises distribution. *Statistical Methodology* 4, 341-353.
- Gerrits, N.M., Epema, A.H., Vanlinge, A., and Dalm, E. (1989). The Primary Vestibulocerebellar Projection in the Rabbit - Absence of Primary Afferents in the Flocculus. *Neuroscience Letters* 105, 27-33.
- Ghosh, K.K., Burns, L.D., Cocker, E.D., Nimmerjahn, A., Ziv, Y., El Gamal, A., and Schnitzer, M.J. (2011). Miniaturized integration of a fluorescence microscope. *Nature Methods* 8, 871-U147.
- Goodman, D.C., and Simpson, J.T. (1961). Functional Localization in Cerebellum of Albino Rat. *Experimental Neurology* 3, 174ff.
- Gravel, C., and Hawkes, R. (1990). Parasagittal organization of the rat cerebellar cortex: direct comparison of Purkinje cell compartments and the organization of the spinocerebellar projection. *The Journal of Comparative Neurology* 291, 79-102.
- Greene, E. (1968). *Anatomy of the rat* (New York: Hafner Pub. Co.).
- Groenewegen, H.J., and Voogd, J. (1977). The parasagittal zonation within the olivocerebellar projection. I. Climbing fiber distribution in the vermis of cat cerebellum. *The Journal of Comparative Neurology* 174, 417-488.
- Hansel, C., Linden, D.J., and D'Angelo, E. (2001). Beyond parallel fiber LTD: the diversity of synaptic and non-synaptic plasticity in the cerebellum. *Nature Neuroscience* 4, 467-475.
- Hantman, A.W., and Jessell, T.M. (2010). Clarke's column neurons as the focus of a corticospinal collary circuit. *Nature Neuroscience* 13, 1233-1239.
- Hawkes, R., Colonnier, M., and Leclerc, N. (1985). Monoclonal-Antibodies Reveal Sagittal Banding in the Rodent Cerebellar Cortex. *Brain Research* 333, 359-365.
- Hobson, J., and McCarley, R. (1972). Spontaneous discharge rates of cat cerebellar Purkinje cells in sleep and waking. *Electroencephalography and Clinical Neurophysiology*, 457-469.
- Hoogland, T.M., De Gruijl, J.R., Witter, L., Canto, C.B., and De Zeeuw, C.I. (2015). Role of Synchronous Activation of Cerebellar Purkinje Cell Ensembles in Multi-joint Movement Control. *Current Biology* 25, 1157-1165.

- Huang, C.-C., Sugino, K., Shima, Y., Guo, C., Bai, S., Mensh, B.D., Nelson, S.B., and Hantman, A.W. (2013). Convergence of pontine and proprioceptive streams onto multi-modal cerebellar granule cells. *eLife* 2, e00400.
- Ito, M. (2001). Cerebellar long-term depression: characterization, signal transduction, and functional roles. *Physiological Reviews* 81, 1143-1195.
- Jansen, J., and Brodal, A. (1940). Experimental studies on the intrinsic fibers of the cerebellum. *The Journal of Comparative Neurology* 73, 267-321.
- Jansen, J., and Brodal, A. (1954). *Aspects of Cerebellar Anatomy* (Oslo: Johan Grundt Tanum Forlag).
- Jeannerod, M., Mouret, J., and Jouviet, M. (1965). [Secondary Effects of Visual Deafferentation on Ponto-Geniculo-Occipital Phase Electrical Activity of Paradoxical Sleep]. *Journal de Physiologie* 57, 255-256.
- Jensen, D.W. (1985). Posture-correlated responses to vestibular polarization in vermal versus intermediate posterior cerebellar cortex. *Experimental Neurology* 88, 629-639.
- Ji, Z., and Hawkes, R. (1994). Topography of Purkinje cell compartments and mossy fiber terminal fields in lobules II and III of the rat cerebellar cortex: spinocerebellar and cuneocerebellar projections. *Neuroscience* 61, 935-954.
- Kara, P., Reinagel, P., and Reid, R.C. (2000). Low response variability in simultaneously recorded retinal, thalamic, and cortical neurons. *Neuron* 27, 635-646.
- Karashima, A., Nakamura, K., Sato, N., Nakao, M., Katayama, N., and Yamamoto, M. (2002). Phase-locking of spontaneous and elicited ponto-geniculo-occipital waves is associated with acceleration of hippocampal theta waves during rapid eye movement sleep in cats. *Brain Research* 958, 347-358.
- Karashima, A., Nakao, M., Katayama, N., and Honda, K. (2005). Instantaneous acceleration and amplification of hippocampal theta wave coincident with phasic pontine activities during REM sleep. *Brain Research* 1051, 50-56.
- Kaufman, L.S., and Morrison, A.R. (1981). Spontaneous and elicited PGO spikes in rats. *Brain Research* 214, 61-72.
- Kitamura, K., and Hausser, M. (2011). Dendritic calcium signaling triggered by spontaneous and sensory-evoked climbing fiber input to cerebellar Purkinje cells in vivo. *The Journal of Neuroscience* 31, 10847-10858.

- Kotchabhakdi, N., and Walberg, F. (1978). Cerebellar afferent projections from the vestibular nuclei in the cat: an experimental study with the method of retrograde axonal transport of horseradish peroxidase. *Experimental Brain Research* 31, 591-604.
- Larsell, O., and Jansen, J. (1967). *The comparative anatomy and histology of the cerebellum* (Minneapolis: University of Minnesota Press).
- Lee, D., Port, N.L., Kruse, W., and Georgopoulos, A.P. (1998). Variability and correlated noise in the discharge of neurons in motor and parietal areas of the primate cortex. *The Journal of Neuroscience* 18, 1161-1170.
- Lee, K.H., Mathews, P.J., Reeves, A.M., Choe, K.Y., Jami, S.A., Serrano, R.E., and Otis, T.S. (2015). Circuit mechanisms underlying motor memory formation in the cerebellum. *Neuron* 86, 529-540.
- Lisberger, S.G., and Fuchs, A.F. (1978a). Role of primate flocculus during rapid behavioral modification of vestibuloocular reflex. I. Purkinje cell activity during visually guided horizontal smooth-pursuit eye movements and passive head rotation. *The Journal of Neurophysiology* 41, 733-763.
- Lisberger, S.G., and Fuchs, A.F. (1978b). Role of primate flocculus during rapid behavioral modification of vestibuloocular reflex. II. Mossy fiber firing patterns during horizontal head rotation and eye movement. *The Journal of Neurophysiology* 41, 764-777.
- Litwin-Kumar, A., and Doiron, B. (2012). Slow dynamics and high variability in balanced cortical networks with clustered connections. *Nature Neuroscience* 15, 1498-1505.
- Loeb, G.E., and Gans, C. (1986). *Electromyography for experimentalists* (Chicago: University of Chicago Press).
- Lundberg, A., and Oscarsson, O. (1956). Functional organization of the dorsal spinocerebellar tract in the cat. IV. Synaptic connections of afferents from Golgi tendon organs and muscle spindles. *Acta Physiologica Scandinavica* 38, 53-75.
- Lundberg, A., and Weight, F. (1971). *Functional Organization of Connexions to the Ventral Spino-Cerebellar Tract*. *Experimental Brain Research*.
- Mandelblat-Cerf, Y., Paz, R., and Vaadia, E. (2009). Trial-to-trial variability of single cells in motor cortices is dynamically modified during visuomotor adaptation. *The Journal of Neuroscience* 29, 15053-15062.
- Mano, N. (1970). Changes of simple and complex spike activity of cerebellar purkinje cells with sleep and waking. *Science (New York, NY)* 170, 1325-1327.

- Manzoni, D., Pompeiano, O., Bruschini, L., and Andre, P. (1999). Neck input modifies the reference frame for coding labyrinthine signals in the cerebellar vermis: a cellular analysis. *Neuroscience* 93, 1095-1107.
- Marchesi, G.F., and Strata, P. (1970). Climbing fibers of cat cerebellum: modulation of activity during sleep. *Brain Research* 17, 145-148.
- Mardia, K.V., and Jupp, P.E. (2000). *Directional statistics* (New York: Wiley).
- Marks, G., Farber, J., Rubinstein, M., and Roffwarg, H. (1980a). Demonstration of Ponto-Geniculo-Occipital the Albino Rat Waves in the Albino Rat. *Experimental Neurology* 666, 648-666.
- Marks, G., Farber, J., and Roffwarg, H.P. (1980b). Metencephalic localization of ponto-geniculo-occipital waves in the albino rat. *Experimental Neurology* 69, 667-677.
- Marr, D. (1969). A theory of cerebellar cortex. *The Journal of Physiology* 202, 437-470.
- Martino, G., Ivanenko, Y.P., Serrao, M., Ranavolo, A., d'Avella, A., Draicchio, F., Conte, C., Casali, C., and Lacquaniti, F. (2014). Locomotor patterns in cerebellar ataxia. *The Journal of Neurophysiology* 112, 2810-2821.
- Matsushita, M., and Hosoya, Y. (1979). Cells of origin of the spinocerebellar tract in the rat, studied with the method of retrograde transport of horseradish peroxidase. *Brain Research* 173, 185-200.
- Matsushita, M., and Wang, C.L. (1987). Projection pattern of vestibulocerebellar fibers in the anterior vermis of the cat: an anterograde wheat germ agglutinin-horseradish peroxidase study. *Neuroscience Letters* 74, 25-30.
- Maynard, E.M., Hatsopoulos, N.G., Ojakangas, C.L., Acuna, B.D., Sanes, J.N., Normann, R.A., and Donoghue, J.P. (1999). Neuronal interactions improve cortical population coding of movement direction. *The Journal of Neuroscience* 19, 8083-8093.
- McCarley, R., Nelson, J., and Hobson, J. (1978). Ponto-Geniculo-Occipital ( PGO ) Burst Neurons : Correlative Evidence for Neuronal Generators of PGO Waves. *Science* 201, 269-272.
- Medina, J.F., and Lisberger, S.G. (2008). Links from complex spikes to local plasticity and motor learning in the cerebellum of awake-behaving monkeys. *Nature Neuroscience* 11, 1185-1192.
- Monier, C., Chavane, F., Baudot, P., Graham, L.J., and Fregnac, Y. (2003). Orientation and direction selectivity of synaptic inputs in visual cortical neurons: a diversity of combi-

nations produces spike tuning. *Neuron* 37, 663-680.

Monsivais, P., Clark, B.a., Roth, A., and Husser, M. (2005). Determinants of action potential propagation in cerebellar Purkinje cell axons. *The Journal of Neuroscience* 25, 464-472.

Moreno-Bote, R., Beck, J., Kanitscheider, I., Pitkow, X., Latham, P., and Pouget, A. (2014). Information-limiting correlations. *Nature Neuroscience* 17, 1410-1417.

Morton, S.M., and Bastian, A.J. (2004). Cerebellar control of balance and locomotion. *The Neuroscientist* 10, 247-259.

Nieuwenhuys, R., Donkelaar, H.J.t., and Nicholson, C. (1998). *The central nervous system of vertebrates* (Berlin; New York: Springer).

Orlovsky, G.N. (1972). Activity of the Purkinje cells during locomotion. *Biofizika* 5, 891-896.

Orlovsky, G.N., Deliagina, T.G., and Grillner, S. (1999). *Neuronal control of locomotion : from mollusc to man* (New York: Oxford University Press).

Oscarsson, O. (1965). Functional Organization of the Spino- and Cuneocerebellar Tracts. *Physiological Reviews* 45, 495-522.

Oscarsson, O. (1979). Functional Units of the Cerebellum - Sagittal Zones and Microzones. *Trends in Neurosciences* 2, 143-145.

Oscarsson, O., and Uddenberg, N. (1964). Identification of a Spinocerebellar Tract Activated From Forelimb Afferents in the Cat. *Acta Physiologica Scandinavica* 62, 125-136.

Ozden, I., Dombeck, D.A., Hoogland, T.M., Tank, D.W., and Wang, S.S.-H. (2012). Widespread state-dependent shifts in cerebellar activity in locomoting mice. *PloS one* 7, e42650.

Palay, S.L., and Chan-Palay, V. (1974). *Cerebellar cortex: cytology and organization* (Berlin, Heidelberg, New York: Springer).

Paxinos, G. (2004). *The rat nervous system, 3rd edn* (Amsterdam; Boston: Elsevier Academic Press).

Pellet, J., and Harlay, F. (1977). [Relations between the unit activity of the vermis cerebelli and the phasic waves of the electrocerebellogram during sleep in chronic cats]. *Archives Italiennes de Biologie* 115, 108-135.

- Pellet, J., Tardy, M.F., Dubrocard, S., and Harlay, F. (1974). [Phasic electrical activity of the cerebellar cortex during sleep and wakefulness]. *Archives Italiennes de Biologie* 112, 163-195.
- Popova, L.B., Ragnarson, B., Orlovsky, G.N., and Grant, G. (1995). Responses of neurons in the central cervical nucleus of the rat to proprioceptive and vestibular inputs. *Archives Italiennes de Biologie* 133, 31-45.
- Precht, W., Volkind, R., and Blanks, R.H. (1977). Functional organization of the vestibular input to the anterior and posterior cerebellar vermis of cat. *Experimental Brain Research* 27, 143-160.
- Ramsay, J.O., and Silverman, B.W. (2005). *Functional data analysis*, 2nd edn (New York: Springer).
- Rancz, E.A., and Husser, M. (2010). Dendritic spikes mediate negative synaptic gain control in cerebellar Purkinje cells. *Proceedings of the National Academy of Sciences of the United States of America* 107, 22284-22289.
- Reiner, A., and Karten, H.J. (1978). A bisynaptic retinocerebellar pathway in the turtle. *Brain Research* 150, 163-169.
- Roberts, T.D.M. (1967). *Neurophysiology of postural mechanisms* (London: Butterworths)
- Sauerbrei, B.A., Lubenov, E.V., and Siapas, A.G. (2015). Structured Variability in Purkinje Cell Activity during Locomotion. *Neuron* 87, 840-852.
- Shambes, G.M., Gibson, J.M., and Welker, W. (1978). Fractured somatotopy in granule cell tactile areas of rat cerebellar hemispheres revealed by micromapping. *Brain Behavior and Evolution* 15, 94-140.
- Shenoy, K.V., Sahani, M., and Churchland, M.M. (2013). Cortical control of arm movements: a dynamical systems perspective. *Annual Review of Neuroscience* 36, 337-359.
- Sherrington, C.S. (1897). Double (antidrome) conduction in the central nervous system. *Proceedings of the Royal Society of London B* 61, 243-246.
- Shik, M.L., and Orlovsky, G.N. (1976). Neurophysiology of locomotor automatism. *Physiological Reviews* 56, 465-501.
- Shik, M.L., Severin, F.V., and Orlovskii, G.N. (1966). [Control of walking and running by means of electric stimulation of the midbrain]. *Biofizika* 11, 659-666.

- Smith, S.S. (1995). Sensorimotor-correlated discharge recorded from ensembles of cerebellar Purkinje cells varies across the estrous cycle of the rat. *The Journal of Neurophysiology* 74, 1095-1108.
- Snyder, R.L., Faull, R.L., and Mehler, W.R. (1978). A comparative study of the neurons of origin of the spinocerebellar afferents in the rat, cat and squirrel monkey based on the retrograde transport of horseradish peroxidase. *The Journal of Comparative Neurology* 181, 833-852.
- Sokoloff, G., Plumeau, A.M., Mukherjee, D., and Blumberg, M.S. (2015a). Twitch-related and rhythmic activation of the developing cerebellar cortex. *The Journal of Neurophysiology* 114, 1746-1756.
- Sokoloff, G., Uitermarkt, B.D., and Blumberg, M.S. (2015b). REM sleep twitches rouse nascent cerebellar circuits: Implications for sensorimotor development. *Developmental Neurobiology* 75, 1140-1153.
- Stecina, K., Fedirchuk, B., and Hultborn, H.R. (2013). Information to cerebellum on spinal motor networks mediated by the dorsal spinocerebellar tract. *The Journal of Physiology* 0, 1-11.
- Thach, W.T. (1968). Discharge of Purkinje and cerebellar nuclear neurons during rapidly alternating arm movements in the monkey. *The Journal of Neurophysiology* 31, 785-797.
- Thomson, D.B., Isu, N., and Wilson, V.J. (1996). Responses of neurons of the cat central cervical nucleus to natural neck and vestibular stimulation. *The Journal of Neurophysiology* 76, 2786-2789.
- Todorov, E., and Jordan, M.I. (2002). Optimal feedback control as a theory of motor coordination. *Nature Neuroscience* 5, 1226-1235.
- Tolbert, D.L., and Gutting, J.C. (1997). Quantitative analysis of cuneocerebellar projections in rats: differential topography in the anterior and posterior lobes. *Neuroscience* 80, 359-371.
- Tolias, A.S., Ecker, A.S., Siapas, A.G., Hoenselaar, A., Keliris, G.A., and Logothetis, N.K. (2007). Recording chronically from the same neurons in awake, behaving primates. *The Journal of Neurophysiology* 98, 3780-3790.
- Udo, M., Matsukawa, K., and Kamei, H. (1981). Simple and Complex Spike Activities of Purkinje Cells During Locomotion in the Cerebellar Vermal Zones of Decerebrate Cats. *Experimental Brain Research* 41, 292-300.
- Valdes, J.L., McNaughton, B.L., and Fellous, J.M. (2015). Offline reactivation of experience-dependent neuronal firing patterns in the rat ventral tegmental area. *The Journal of Neu-*

rophysiology 114, 1183-1195.

Van Lieshout, M., and Baddeley, A.J. (1996). A nonparametric measure of spatial interaction in point patterns. *Statistica Neerlandica* 50, 344-361.

Vinueza Veloz, M.F., Zhou, K., Bosman, L.W., Potters, J.W., Negrello, M., Seepers, R.M., Strydis, C., Koekkoek, S.K., and De Zeeuw, C.I. (2014). Cerebellar control of gait and interlimb coordination. *Brain Structure and Function*.

Voogd, J., Pardoe, J., Ruigrok, T.J.H., and Apps, R. (2003). The distribution of climbing and mossy fiber collateral branches from the copula pyramidis and the paramedian lobule: congruence of climbing fiber cortical zones and the pattern of zebrin banding within the rat cerebellum. *The Journal of Neuroscience* 23, 4645-4656.

Wierzynski, C.M., Lubenov, E.V., Gu, M., and Siapas, A.G. (2009). State-dependent spike-timing relationships between hippocampal and prefrontal circuits during sleep. *Neuron* 61, 587-596.

Wilson, M.A., and McNaughton, B.L. (1994). Reactivation of hippocampal ensemble memories during sleep. *Science* 265, 676-679.

Wimmer, R.D., Schmitt, L.I., Davidson, T.J., Nakajima, M., Deisseroth, K., and Halassa, M.M. (2015). Thalamic control of sensory selection in divided attention. *Nature* 526, 705-709.